NAVAL POSTGRADUATE SCHOOL
MONTEREY, CALIFORNIA

THESIS

IONIAN SEA SURFACE TEMPERATURE: SATELLITE AND DRIFTER OBSERVATIONS, MAY TO OCTOBER, 1995

by

Jeffrey M. Leitz

September 1999

Thesis Advisor: Pierre-Marie Poulain
Second Reader: Philip A. Durkee

Aproved for public release; distribution is unlimited.

REPORT DOCUMENTATION PAGE

Form Approved
OMB No. 0704-0188

1. AGENCY USE ONLY *(Leave blank)*	2. REPORT DATE	3. REPORT TYPE AND DATES COVERED
	September 1999	Master's Thesis

4. TITLE AND SUBTITLE
IONIAN SEA SURFACE TEMPERATURE: SATELLITE AND DRIFTER OBSERVATIONS, MAY TO OCTOBER, 1995

5. FUNDING NUMBERS

6. AUTHOR(S)
Leitz, Jeffrey M.

7. PERFORMING ORGANIZATION NAME(S) AND ADDRESS(ES)
Naval Postgraduate School
Monterey, CA 93943-5000

8. PERFORMING ORGANIZATION REPORT NUMBER

9. SPONSORING / MONITORING AGENCY NAME(S) AND ADDRESS(ES)

10. SPONSORING / MONITORING AGENCY REPORT NUMBER

11. SUPPLEMENTARY NOTES
The views expressed in this thesis are those of the author and do not reflect the official policy or position of the Department of Defense or the U.S. Government.

12a. DISTRIBUTION / AVAILABILITY STATEMENT
Approved for public release; distribution is unlimited.

12b. DISTRIBUTION CODE

13. ABSTRACT *(maximum 200 words)*

The Ionian Sea is the central basin of the Mediterranean Sea and has been the subject of various oceanographic studies since the 19th century. Substantial changes in water properties (such as temperature), both spatially and temporally (seasonal) occur as a result of extreme forcings by the local winds and by the inflow of cool and less saline Atlantic waters. In recent years, extensive measurements have been made, primarily through remote sensing techniques. In particular, satellite infrared data were used to study the surface thermal features and associated circulation.

In order to improve upon previous results, this study focuses on a period of 6 months (May to October, 1995) in which the full resolution (1.25x1.25 km) satellite images are used to describe and study the variability of the sea surface temperature (SST) and circulation from meso- (days) to seasonal (months) scales. The satellite infrared temperatures are compared to simultaneous and collocated in-situ drifter temperature measurements. They are corrected by removing biases obtained by regression analysis. The corrected images are used to produce maps representing daily, three-day, weekly and monthly Ionian SSTs. Selected SST composites augmented with drifter track and wind field overlays disclose important quantitative features of the Ionian surface waters, such as upwelling events in the Straits of Otranto and of Sicily, and off the African Coast. The spatial structure and temporal variability of the surface fields are presented and discussed.

14. SUBJECT TERMS	15. NUMBER OF PAGES
Ionian Sea, Oceanography, Remote Sensing, Sea Surface Temperature, Lagrangian Drifters	106
	16. PRICE CODE

17. SECURITY CLASSIFICATION OF REPORT	18. SECURITY CLASSIFICATION OF THIS PAGE	19. SECURITY CLASSIFI- CATION OF ABSTRACT	20. LIMITATION OF ABSTRACT
Unclassified	Unclassified	Unclassified	UL

NSN 7540-01-280-5500

Standard Form 298 (Rev. 2-89)
Prescribed by ANSI Std. 239-18

Approved for public release; distribution is unlimited.

IONIAN SEA SURFACE TEMPERATURE: SATELLITE AND DRIFTER OBSERVATIONS, MAY TO OCTOBER, 1995

Jeffrey M. Leitz
Lieutenant, United States Navy
B.S., Georgia Institute of Technology, 1992

Submitted in partial fulfillment of the
requirements for the degree of

MASTER OF SCIENCE IN PHYSICAL OCEANOGRAPHY

from the

NAVAL POSTGRADUATE SCHOOL
September 1999

Author: 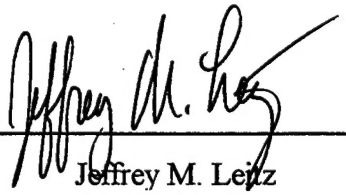
Jeffrey M. Leitz

Approved by: 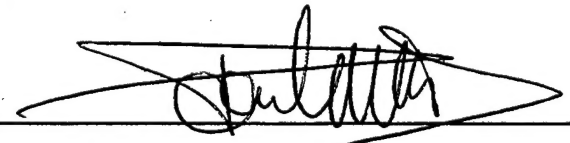
Pierre-Marie Poulain, Thesis Advisor

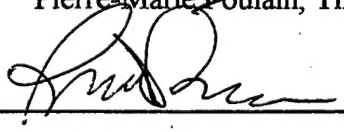
Philip A. Durkee, Second Reader

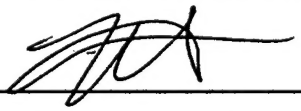
Roland W. Garwood, Chairman
Department of Oceanography

ABSTRACT

The Ionian Sea is the central basin of the Mediterranean Sea and has been the subject of various oceanographic studies since the 19th century. Substantial changes in water properties (such as temperature), both spatially and temporally (seasonal) occur as a result of extreme forcings by the local winds and by the inflow of cool and less saline Atlantic waters. In recent years, extensive measurements have been made, primarily through remote sensing techniques. In particular, satellite infrared data were used to study the surface thermal features and associated circulation.

In order to improve upon previous results, this study focuses on a period of 6 months (May to October, 1995) in which the full resolution (1.25x1.25 km) satellite images are used to describe and study the variability of the sea surface temperature (SST) and circulation from meso- (days) to seasonal (months) scales. The satellite infrared temperatures are compared to simultaneous and collocated in-situ drifter temperature measurements. They are corrected by removing biases obtained by regression analysis. The corrected images are used to produce maps representing daily, three-day, weekly and monthly Ionian SSTs. Selected SST composites augmented with drifter track and wind field overlays disclose important quantitative features of the Ionian surface waters, such as upwelling events in the Straits of Otranto and of Sicily, and off the African Coast. The spatial structure and temporal variability of the surface fields are presented and discussed.

TABLE OF CONTENTS

LIST OF FIGURES

LIST OF TABLES

ACKNOWLEDGEMENTS

The author would like to thank a number of people for their assistance in the completion of this thesis. First and foremost, Dr. Pierre-Marie Poulain for his guidance. His assistance greatly increased my understanding in a topic that cap-stoned my studies here at the Naval Postgraduate School. Also, Dr. Philip A. Durkee, my second reader, who provided timely and thoughtful recommendations to the thesis manuscript. In addition, the following organizations provided essential data, expertise and assistance during my research: the NATO SACLANT Undersea Research Centre, La Spezia, Italy provided the AVHRR and drifter data used in this study; the Satellite Oceanography Laboratory, University of Hawaii processed the AVHRR data and provided technical assistance; and the Naval Oceanographic Office (NAVOCEANO), Stennis Space Center, Mississippi, USA, gave us the orographically rotated NORAPS data used for generating wind overlays. LT Jason A. Vogt, whose suggestion of a thesis advisor and topic was a corner stone of my thesis. Mr. Mike Cook is acknowledged for his MATLAB expertise, and some inspirational computer coding, and Ms. Donna Burych for general computer assistance.

I. INTRODUCTION

The Ionian Sea is the central basin of the Mediterranean Sea. It represents the transitional basin between the western Mediterranean and the Levantine Sea, source of the highly saline water that flows from the Mediterranean Sea to the Atlantic Ocean. Subject to robust seasonal changes, the Ionian Sea has been the subject of many experiments to collect data about its structure. More recently, remote sensing, using satellite data collection, has allowed synoptic observations of sea surface temperatures throughout the year. This provides a wealth of data, not easily analyzed due its enormous size. Recent papers have examined the Eastern Mediterranean using weekly averages of sea surface temperatures with reduced (18x18 km) spatial resolution (Marullo et al., 1999).

A shortened time period from May to October 1995 is examined in this thesis so that the full resolution (1.25x1.25 km) of NOAA satellite images can be used. Processed data were corrected for bias by using in situ drifter temperatures. This was accomplished using linear regression analyses of simultaneous and collocated drifter and satellite sea surface temperatures. Drifters also provided verification of surface currents by overlaying

their tracks on various sea surface temperatures composite images. Weekly and monthly sea surface temperature composite images of the Ionian Sea were generated, using the available corrected satellite images. They provide a clear visual representation of mesoscale and sub-basin structures in the Ionian Sea including substantial seasonal variability.

Of particular interest to United States Navy is the near real-time processing and distribution of these images as tools for forecasting the presence of thermal fronts. These fronts are known for their effects on sound propagation in the water column.

This thesis is organized into five chapters. Chapter II provides a detailed background to allow the reader a better understanding of the regional characteristics, the basis for this study, and the tools that were required to complete it. Chapter III discusses the means with which data were collected, organized, manipulated, and presented. The complete results of these methods for the time period of May to October, 1995 are presented in Chapter IV. Discussion, summaries and conclusions make up Chapter V.

II. BACKGROUND

This chapter describes the geography/topography, weather, surface thermal structure and circulation of the Ionian Sea.

A. GEOGRAPHY/TOPOGRAPHY

The Mediterranean Sea (Figure II-1) is bounded by the coasts of southern Europe, northern Africa and western Asia. With a mean depth of 1500 m, it is easily divided into an eastern and western half by the shallow Straits of Sicily, separating the European and African continents. It has limited communication with the Atlantic Ocean, through the Straits of Gibraltar.

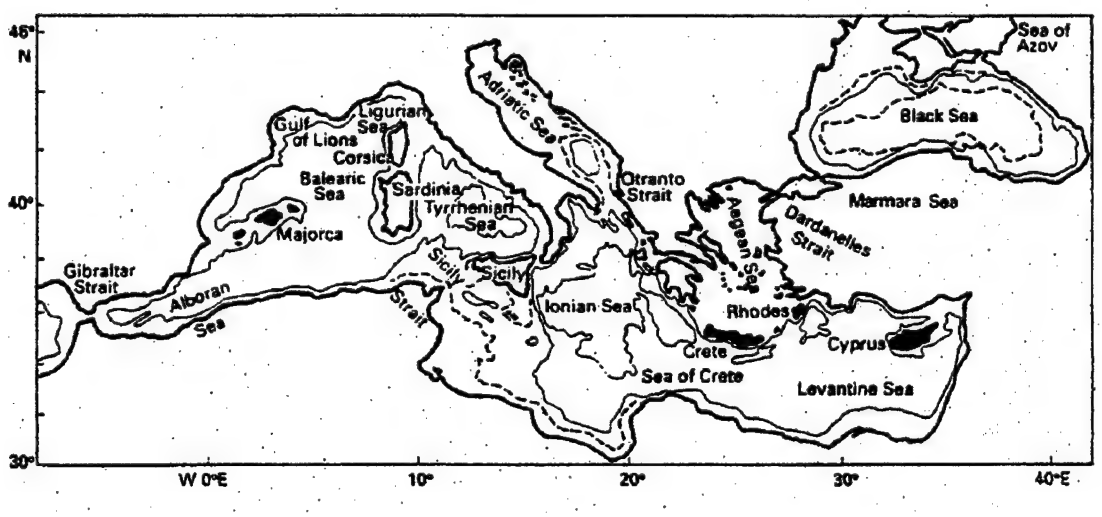

Figure II-1. Mediterranean Sea, showing nonmenclature of the major sub-basins and Straits (from Godfrey and Tomaczak, 1994).

The Ionian Sea is a large semi-enclosed deep basin of the eastern Mediterranean Sea (Figure II-2). Defined by the Sicily Straits, Otranto Straits and the Cretan Passage, the Ionian Sea connects the Levantine, Adriatic and Tyrrhenian Seas. In the Sicily Straits, the continental shelves of Europe and Africa combine to create a sill depth of nearly 400 m. Off the southern tip of Sicily, from the Adventure Bank and Malta Shelf, moving directly south, to the Tunisian Shelf, off the northern African coast, and moving east, the sea floor rapidly slopes to the deepest depths of the Ionian basin, approximately 3800 m in the center of the Ionian Sea. Continuing east, the sea-floor gradually decreases in depth, to approximately 2000 m, then transitioning into the Cretan Passage. Starting at the Otranto Straits, at the mouth of the southern Adriatic Sea, and moving directly south towards the African coast, the sea floor quickly descends to 2500 me, then gradually increases in depth to 3800 m. Moving south from the center of the Ionian Sea, the sea floor gradually decreases in depth until reaching the northern African coast.

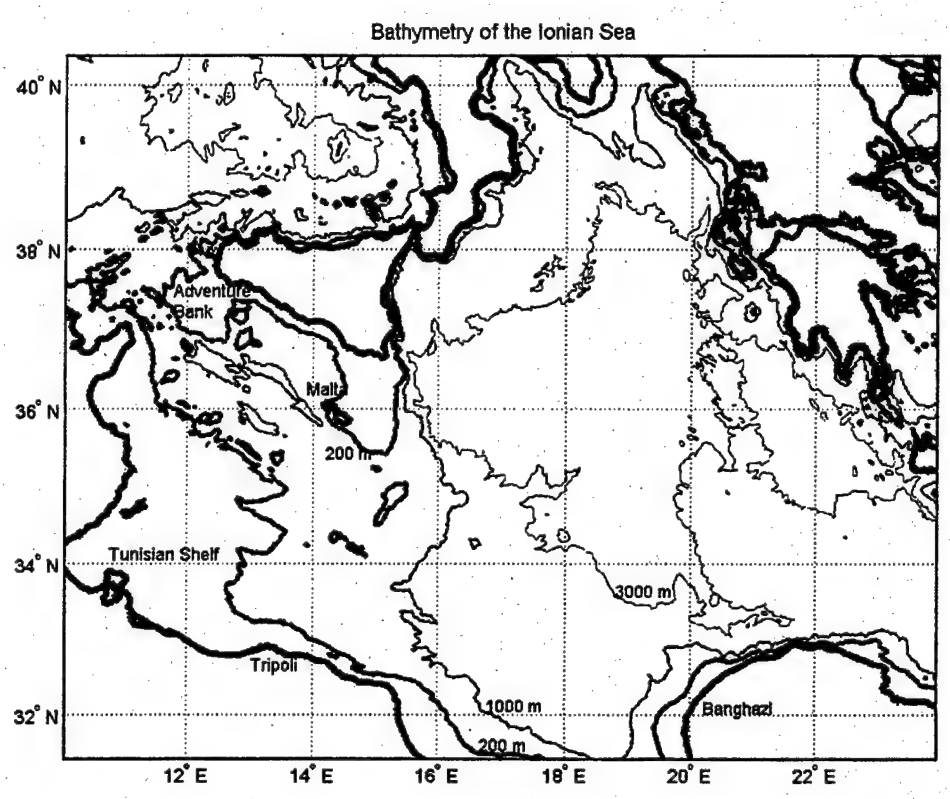

Figure II-2. Bathymetry of the Ionian Sea.

B. CIRCULATION

As a concentration basin, the Mediterranean Sea provides a large outflow of highly saline water to the Atlantic Ocean through the Strait of Gibraltar. This is due to the annual evaporation of water being greater than precipitation. The three main sources of water is river out flow from the Adriatic Sea and Black Sea, and cold water from the Atlantic Ocean, flowing near the surface through the Straits of Gibraltar. The cold Atlantic water flows

east forming the Algerian current. Before entering the eastern Mediterranean Sea, Atlantic water moves through the western Mediterranean Sea, then into the Sicily Straits, becoming Modified Atlantic Water (MAW), (Malanotte-Rizzoli et al., 1997).

Because evaporation exceeds precipitation in the Mediterranean Sea, the flow of water is driven by density differences between the surface and sub-surface water. More saline surface water flows down the water column, creating large convective circulation. Due to this density driven flow, Atlantic water moves into the Mediterranean Sea on the surface, while more saline Mediterranean water flows into the Atlantic Ocean underneath the in-flow (Godfrey and Tomaczak, 1994).

The eastern Mediterranean is comprised of three basin-scale thermohaline cells. The Adriatic Sea, with its surplus of freshwater from river outflow, supplies the eastern Mediterranean with its deep internal cell of cold water, the eastern Mediterranean Deep Water (EMDW), which flows to the bottom of the Ionian and Levantine Seas. Recent studies show that the Aegean Deep Water also supplies water to the EMDW (Roether et al., 1998). The second cell of water involves the transport of MAW from the western Mediterranean, through the Sicily Straits and Ionian Sea, into the Levantine Sea. The final cell of water is the

highly saline Levantine Intermediate Water (LIW). LIW is formed in the Levantine Sea and flows westward, underneath MAW on its path to the Atlantic Ocean (Malanotte-Rizzoli et al., 1997).

The near surface circulation of the Ionian Sea is primarily dominated by the Atlantic-Ionian Stream (AIS), formed from cool Atlantic water flowing into the eastern Mediterranean Sea through the Sicily Strait (Figure II-3). The winter (November to April) zonal pattern is characterized by cold and warm water in the northern and southern Ionian Sea, respectively. This zonal pattern is due largely to the path of the AIS travelling eastward from the Sicily Strait towards the African coast, becoming the North African Current. The North African Current flows directly towards the Cretan Passage, except when the Cretan Cyclone, off the south coast of Crete, is present. Then the North African Current moves closely along the African coast. From June to October, the AIS forms a strong thermal front east of the Strait of Sicily (Malta Front). The AIS moves to the north-north east along the Italian coast, then down the western Greek Peninsula, passing the warm Pelops Anticyclone. Passing further south, the AIS flows around the cold Cretan Cyclone, off the southwest coast of Crete. The warm Pelops Anticyclone and cold Cretan Cyclone are of a transient nature, and typically loose their sea surface

temperature signature in the summer due to the development of a strong thermocline (Matteoda and Glenn, 1996). Finally, the AIS becomes the southward-flowing Mid-Mediterranean Jet (MMJ) before entering the Cretan Passage and transitioning to the Levantine Sea (Robinson et al., 1999). Using satellite-tracked drifters, these sub-basin and mesoscale flow structures have been confirmed by Poulain (1998).

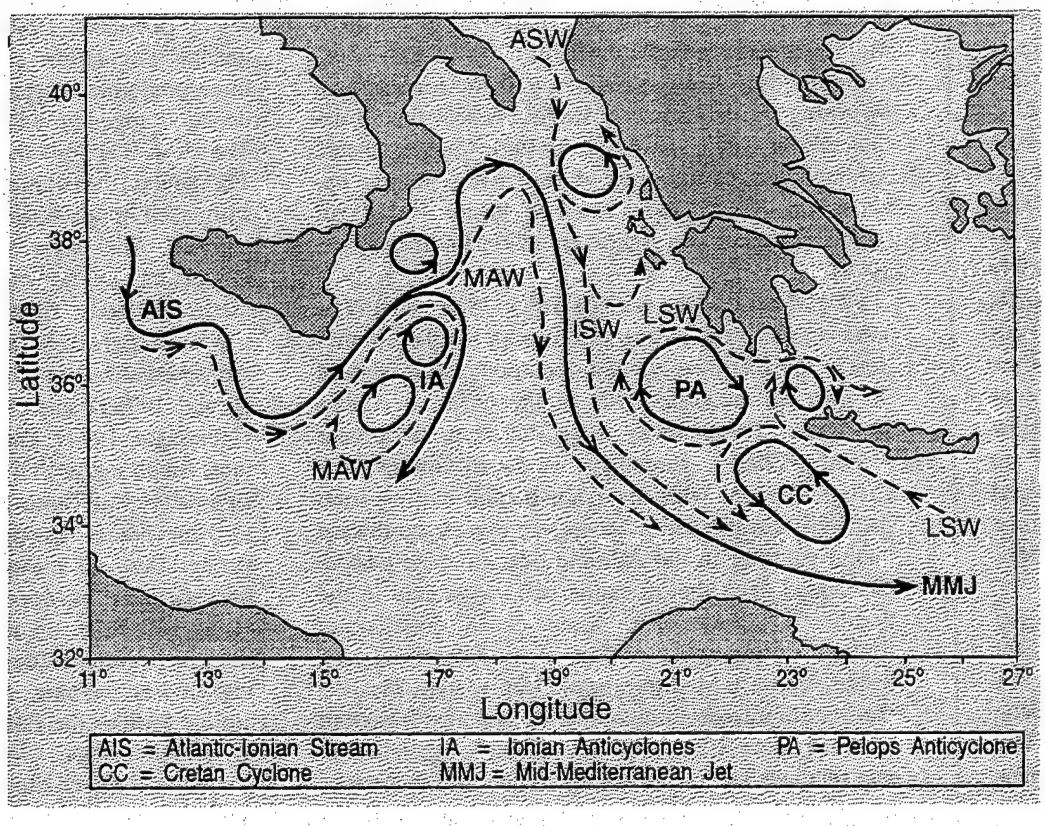

Figure II-3. Surface Mesoscale features of the Ionian Sea (from Malanotte-Rizzoli et al., 1997).

C. WEATHER

The Mediterranean Sea's characteristic of evaporation exceeding precipitation is largely caused by prevailing dry northwest winds and high percentage of cloud free days (Pickard and Emery, 1990). This variability of wind forcing combines with the relative isolation of the Mediterranean Sea, creating an area where salinity difference is more important in forcing currents, as the rapid cooling of saline surface water by northern winds demonstrates (Matteoda et al., 1996). In the western Mediterranean, mistral winds blow from the northwest near the coast of France. Reaching speeds up to 70 miles per hour and lasting from a few days to a week, these cold and dry winds can reach the Straits of Sicily and the eastern Mediterranean year-round. The spring (April, May and June) is characterized by calm wind areas (Philippe and Harang, 1982). The summer (July, August and September) brings strong northerly winds (Etesian winds or Meltemi) over the east Aegean Sea and winds from the east along the North African coast. Winds shift in autumn (October, November and December), transitioning from the east in summer, to westerly in winter. In the Aegean and Adriatic Seas, the Etesian winds become erratic, giving rise to winds from the

south (Sirocco). The Sirocco winds are either dry or very humid, and blow mainly in spring and autumn (Huxley, 1962).

D. SEA SURFACE TEMPERATURE

The sea surface temperature (SST) of the Ionian Sea is characterized by a strong seasonal variability. The Ionian surface thermal field is characterized by a zonal SST distribution between November and April, transitioning during May to a meridional SST distribution (Marullo et al., 1999). The meridional SST distribution dominates from June to September, before a rapid transition to the zonal SST distribution occurs in October. Marullo et al. (1999) used NASA Ocean Data System/Multi-Channel Sea Surface Temperature (NODS/MCSST) data. The data were obtained from Advanced Very High-Resolution Radiometer (AVHRR) instruments aboard National Oceanic and Atmospheric Administration (NOAA) satellites. With low resolution (18x18 km) and weekly averages, these observations were only able to describe large, basin-wide structures, although covering one decade's worth of SST data. The mean SST of the Eastern Mediterranean for the period 1983-1992, is presented in Figure II-4.

Satellite observations by Philippe and Harang (1982), using AVHRR data from April 1979 to March 1981, show that in

May only weak temperature fronts exist, due to the cooling effects of the winter season. Large warm patches of water are observed when calm wind areas are combined with strong surface diurnal heating. During the summer, temperature vertical stratification is strongest and the African current in association with strong temperature fronts. Upwelling occurs in the area south of Sicily. Associated with prevailing westerly winds, upwelling continues until the beginning of winter (Manzella et al., 1990). In the southern Adriatic Sea and Strait of Otranto area, north and northeasterly winds cause upwelling (Gacic et al., 1997). This causes currents to meander, rather than follow the usual northern bound circulation pattern (Poulain, 1999). Also, along the African coast, upwelling occurs when winds blow from the east. Autumn is a transitional time for sea surface temperatures. Winds that typically blow from the east in summer, shift from the west in winter during late September and October. The sea surface temperature fronts become meridional. In the Ionian Sea, the temperature front meanders along the Italian Peninsula. Here, summer and winter front patterns may be alternatively observed. Winter temperature patterns include anticyclonic eddies in the Ionian Sea, with zonal patterns associated with the AIS flowing through the Strait of Sicily (Marullo et al., 1999; Philippe and Harang, 1982).

Two semipermanent SST features are located within or near the Ionian Sea (Figure II-3). They are the Cretan Cyclone off the southwest coast of Crete, and the Pelops Anticyclone off the southwest coast of Greece. The Cretan Cyclone is a cold core eddy that forms from water originating from the Aegean Sea, between July and January. The Pelops Anticyclone is a warm core eddy that forms between December and April.

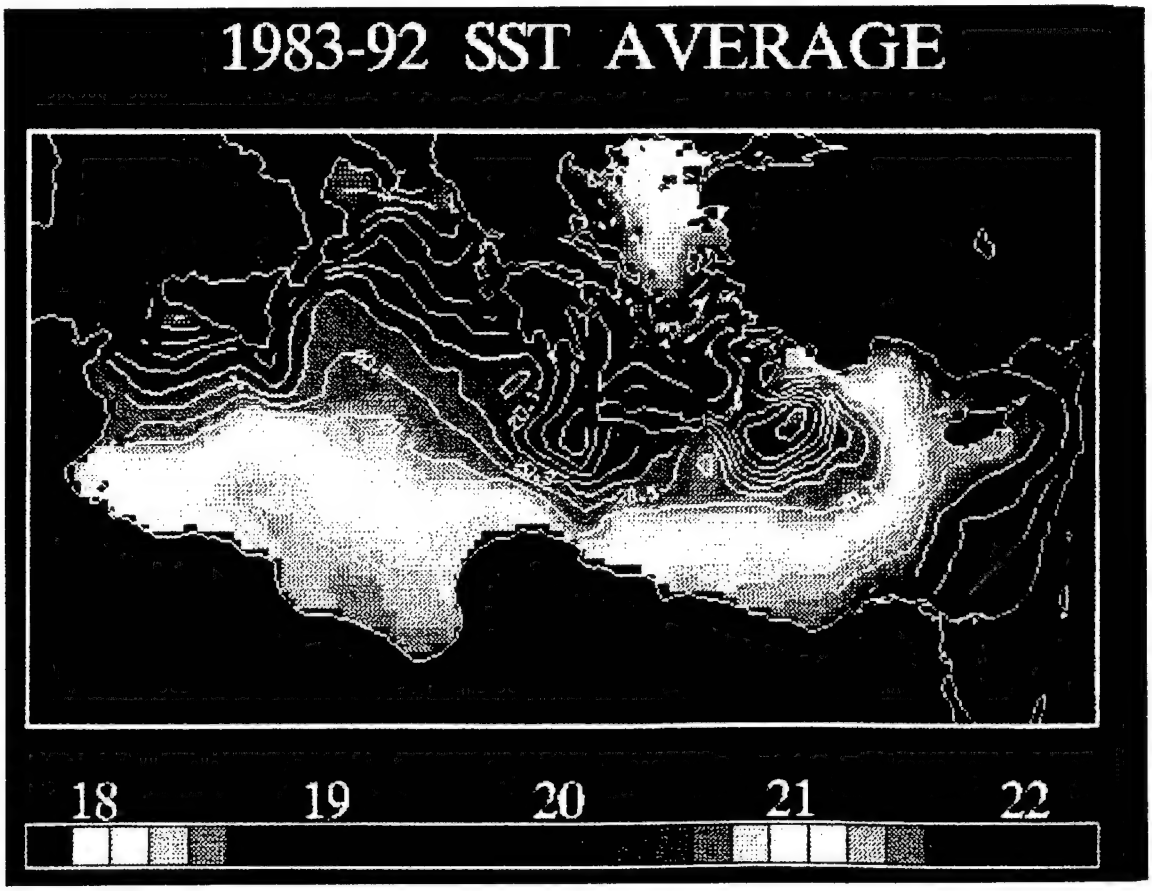

Figure II-4. Time average of the sea surface temperature from the entire time series (1983-92). Temperatures are in °C (from Marullo et al., 1999).

III. DATA AND METHODS

A. DATA

A series of Advanced Very High-Resolution Radiometer (AVHRR) satellite images from May to October 1995 were processed, then compared with available drifter data from corresponding dates and times.

1. Sea Surface Temperature (SST)

National Oceanic and Atmospheric Administration (NOAA) satellites provide remote observations of the earth's surface and atmosphere from space. From an altitude of approximately 830 km, they cover a swath 2400 km wide, generating a surface spatial resolution of 1.1 km at nadir. As Polar Operational Environmental Satellites (POES), these NOAA satellites have a north-south orbit, with orbits of approximately 100 minutes in period. NOAA 9 (Figure III-1a) and NOAA 12 (Figure III-1b) provides early morning (6:00-9:00 AM GMT) and evening (5:00-9:00 PM GMT) satellite images, while NOAA 14 (Figure III-1c) delivers 1:00 AM and 12:00 PM (GMT) images (Lillesand and Kiefer, 1994).

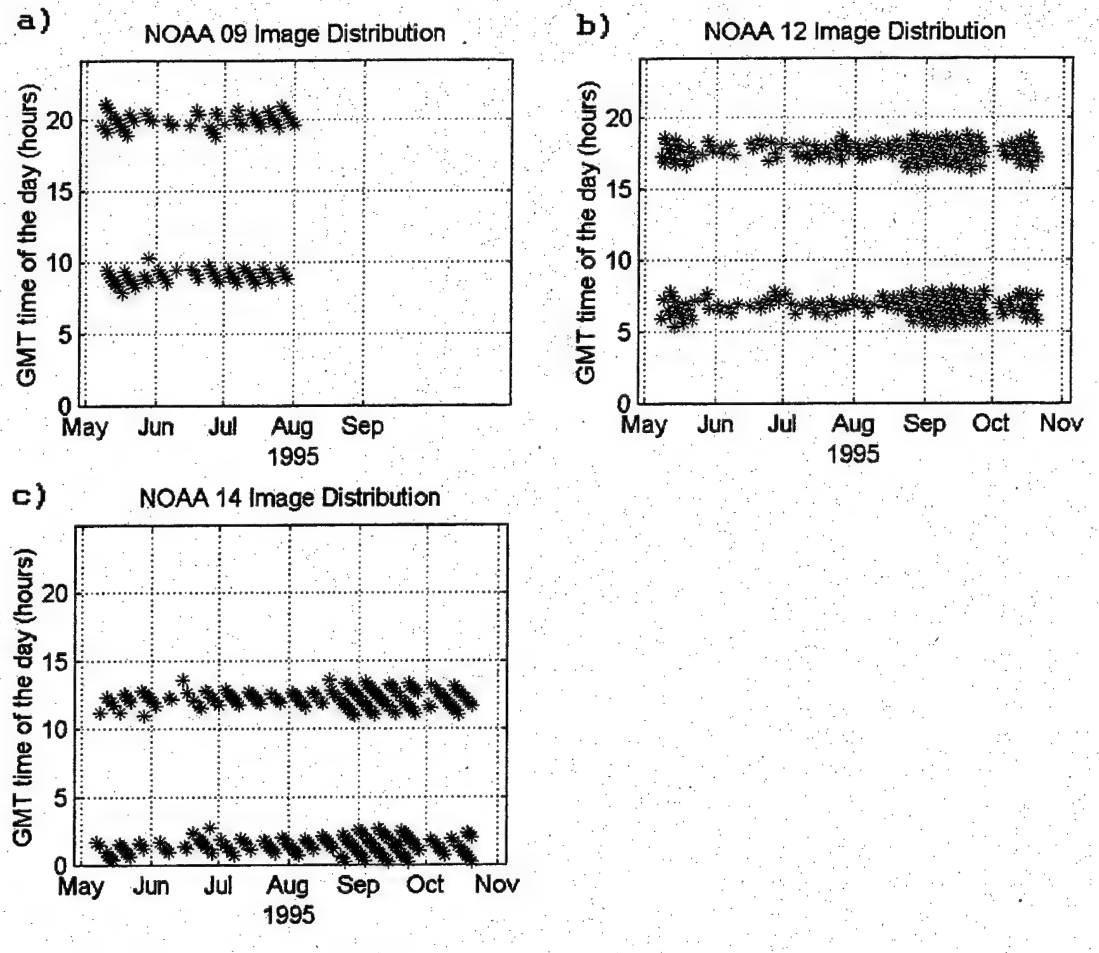

Figure III-1. Distribution plot of image vs. time of day (GMT) for (a) NOAA 9, (b) NOAA 12, and (c) NOAA 14.

a) Multichannel Sea Surface Temperature (MCSST)

Carried aboard NOAA satellites, AVHRR sensors provide 5 discrete channels of data between the visible (channel 1), near-infrared (channels 2 & 3), and thermal infrared (channels 4 & 5) portions of the electromagnetic spectrum. Using the Multichannel Sea Surface Temperature (MCSST) split window equation, SST's may be determined from

AVHRR data as describe by McClain et al. (1985). The MCSST equation has the form:

$$MCSST = a * T_4 + b * (T_4 - T_5) + c * (T_4 - T_5) * (\sec(\theta) - 1) + d$$

where, T_4 and T_5 are channel 4 and 5 brightness temperatures in °C, θ is the satellite zenith angle, and the variables (a, b, c and d) are linear regression coefficients (see Table 1) provided by NOAA for day and night computations.

SATELLITE	a	b	c	d	REMARK
NOAA-9	0.973100	2.635300	0	265.479	Same day and night
NOAA-12	0.963563	2.579211	0.242598	263.006	Day
	0.967077	2.384376	0.480788	263.940	Dusk, dawn, night
NOAA-14	1.017342	2.139588	0.779706	278.430	Day
	1.029088	2.275385	0.752567	282.240	Dusk, dawn, night

Table 1. MCSST Algorithm Coefficients.

The MCSST algorithm corrects for the absorption/emission by atmospheric water vapor. Comparisons between MCSST derived SST's and in-situ (ships, moored buoys, and drifting buoys) SST's by Strong and McClain (1984) reveal RMS differences of 1.81, 1.05, and 0.68 °C, respectively.

The NOAA-9 satellite MCSST coefficients were no longer maintained by NOAA, therefore the SST's derived from NOAA-9 AVHRR data may vary from same day images of NOAA 12 and 14 by a few degrees C (Anonymous, 1998).

b) Image Processing

AVHRR data from NOAA 9, NOAA 12 and NOAA 14 were received and archived on magnetic tape aboard NRV Alliance and at NATO SACLANT Undersea Research Centre, La Spezia, Italy (Anonymous, 1998). These data were then processed at the University of Hawaii Satellite Oceanography Laboratory. Raw AVHRR data were recorded as raw black and white GIF images. Since MATLAB is unable to read GIF images, data were converted to XWD binary files, which could be converted into 8-bit binary arrays for analysis using the following linear mapping:

$$byte\_value = (temperature\_°C - 5) * 10$$

$$temperature\_°C = \frac{byte\_value}{10} + 5$$

The University of Hawaii Satellite Oceanography Laboratory also generated mask GIF images using a variety of tests for cloud detection and other contaminating effects,

and using the geographical extension of land masses (see Table 2).

Test number/Bit test	Test	Remarks
1	Sun reflection > 25°	
2	T_{min} < SST < T_{max}	climatology
3	Std dev T_4 <= 0.3 °C	
4	Std dev Ch 2 <= 0.2 °C	Daytime only
5	Abs(T_3 - T_4) <= 3.0°C	
6	Land mask	
7	Ch1/Ch2 >= 1.35	Daytime only

Table 2. Mask test characteristics (from Anonymous, 1998).

These six tests are designed to identify the contaminated pixels, which might affect satellite-derived SST accuracy. The reflection of sunlight on the sea surface can cause a decrease in the ratio between channel 1 and channel 2. Over these areas, the channel 3 values are much larger than channel 4. This could also result from the presence of low, warm clouds (fog) or high cirrostratus. This does not allow the determination of a clear or cloudy pixel. Therefore, bit test one flags all pixels where the sun reflection angle are less than 25°, allowing the selective use of the fifth and seventh bit tests.

Bit test 2 compares the pixel temperature to an expected temperature based on regional climatology. This climatology was generally not used to mask the SST images for the applications presented in this thesis because the temperature limits turned out to be too stringent. The variation in temperatures due to uneven cloud-top heights of convective clouds is the basis of bit test 3. Bit test 4 is a textural test that looks for clouds based on their tops having a non-uniformity that causes variations in the reflectance. Bit test 5 detects stratiform clouds based on the differences between the infrared channels. Land is masked by bit test 6, and accounts for 25.45% of all pixels in a single image. Bit test 7 compares the radiance ratio of the visible to near-infrared (channels 1 and 2) for pixels where the mean sun zenith angle is less than 80°.

The results from the cloud tests were saved as separate GIF images; they were converted to XWD binary files for analysis and application to their corresponding sea surface temperature XWD files. The mask XWD files were read to determine the pass/failure status of each bit test for each pixel.

2. Drifters

The recent use of disposable drifters capable of providing surface temperature measurements and location has been a significant development in studying surface currents and temperatures. Drifters released in the Adriatic and Ionian Seas have provided global descriptions of their surface circulation, confirming major current patterns, and revealing influences of seasonal variability (Poulain, 1998). Drifters from the Adriatic Sea were mostly released from the eastern side of the Strait of Otranto from December 1994 to October 1995, as part of the NATO SACLANT Otranto Gap project (Poulain, 1999). Drifters were also released into the Ionian Sea from the Sicily Straits.

The drifters (see Figure III-2) are constructed of a one-meter cylinder with four vertically oriented vanes along the length of the cylinder. The drag-producing vanes, at 90° intervals around the circumference of the cylinder, allow the drifter to flow with surface currents and provide valuable speed and direction data. Inside the cylinder, a thermistor is positioned approximately 40 cm below the sea surface. It provides temperature readings ranging from -5 to 39 °C, accurate to within ±0.1 °C. An antenna, extending from the top of the drifter, permits data transmission (at 90-second intervals) of SST's to over- flying ARGOS equipped

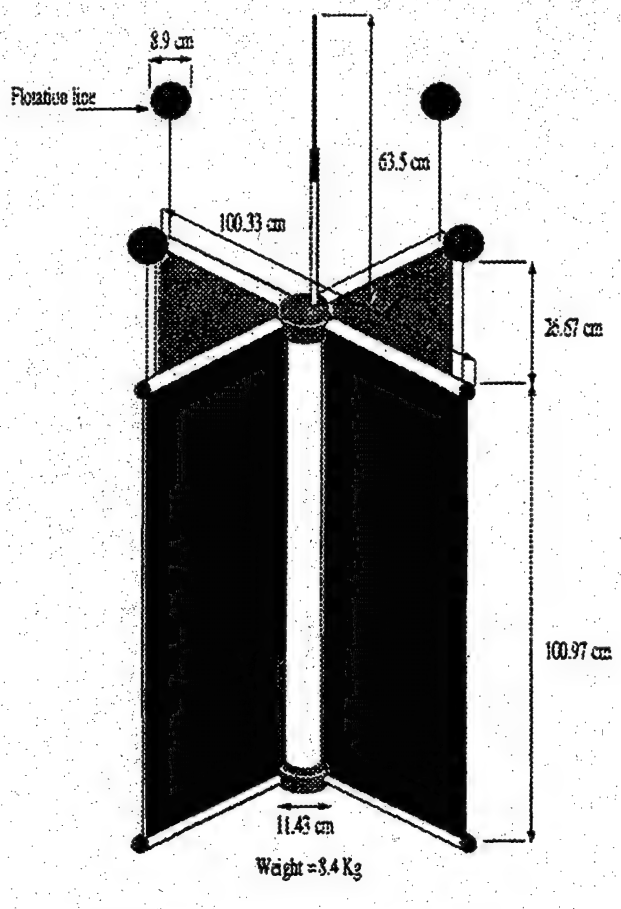

Figure III-2. Schematic diagram of the surface drifter used. The drifter design is similar to the CODE drifter. Four drag producing vanes provide adherance to the water, whereas a small antenna protrudes above sea level for satellite tracking and SST data transmission (from Poulain, 1999).

NOAA satellites. Geographical location of drifters is determined by their Doppler frequency shift of the transmitting fixed-frequency signal (401.65 MHz), to an accuracy of a few hundred meters (Poulain, 1999). Drifter data were processed to obtain low-pass filtered (36 hour cut-off) series of latitude and longitude, velocity and sea

surface temperature at 6 hour intervals (Poulain, 1998, 1999). Figure III-3 plots the drifter trajectory for drifters in the Ionian Sea during the time of the study.

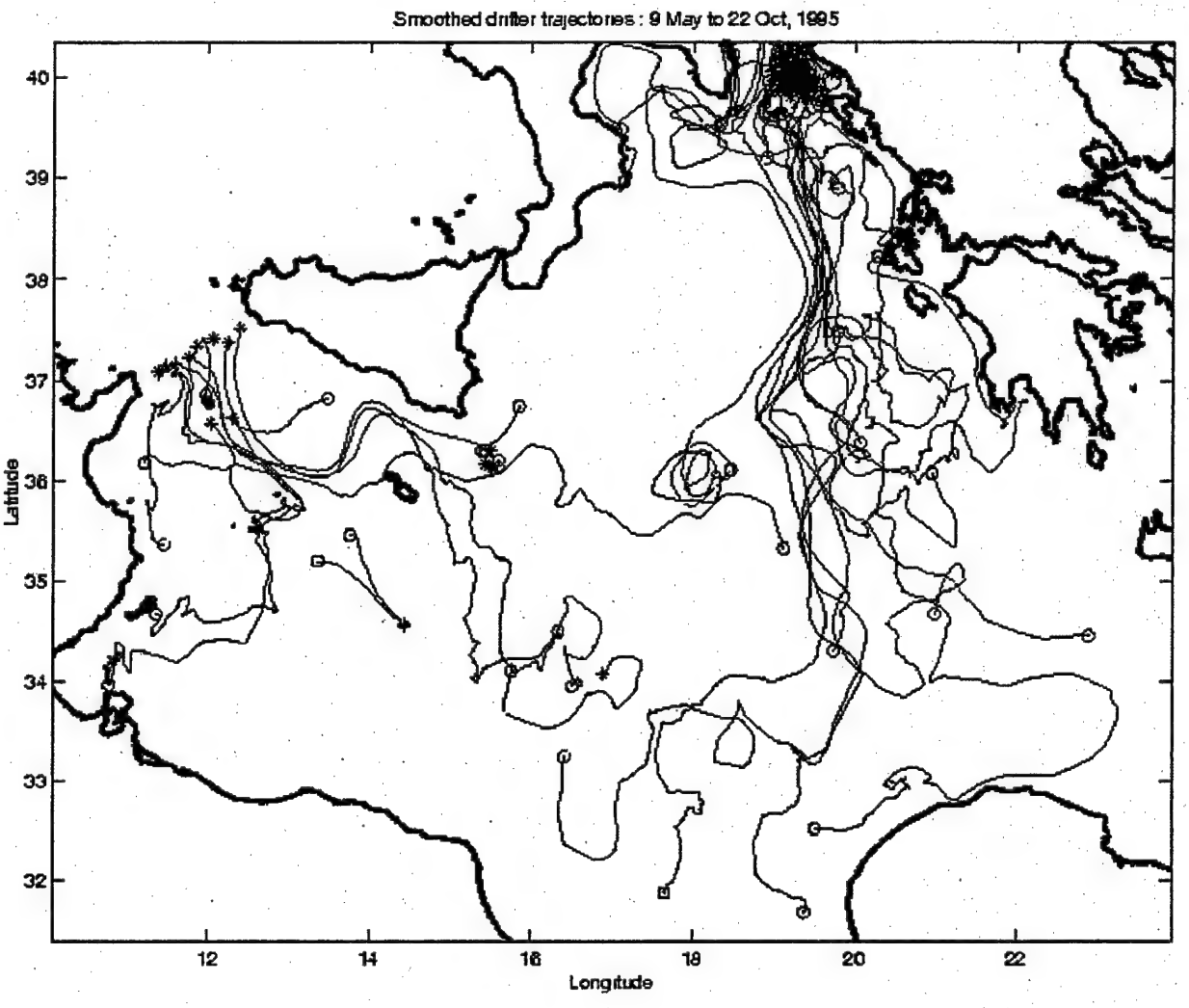

Figure III-3. Plot of drifter trajectories in the Ionian Sea from 9 May to 22 October, 1995. Star and open circle symbols denote the first (usually deployment) and last locations of the drifters, respectively.

In Figure III-3, the primary release points are seen at the Otranto and Sicily straits. The drifters released in the

Sicily and Otranto Straits closely follow the observed path associated with the Atlantic-Ionian Stream and Mid-Ionian Jet, respectively (Figure II-3).

3. Wind Product

Information on the near-surface wind speed and direction over the Mediterranean was obtained from the Navy Operational Regional Atmospheric Prediction System (NORAPS). The horizontal resolution of the NORAPS winds is 45 km. In order to take into account the significant control of the orography of Mediterranean islands and nearby mountains on surface winds, the NORAPS winds were orographically steered using an atmospheric boundary layer (Horton et al., 1997). An example of the steered NORAPS wind field is shown in Figure III-4 for 17 August 1995. On that particular day, three major Mediterranean winds are outstanding: the northwesterly Mistral extending from the south of France, crossing the Western Basin and continuing to the Ionian via the Straits of Sicily; the northeasterly Bora in the northern Adriatic and the northerly Etesian winds over the Aegean and Cretan Seas.

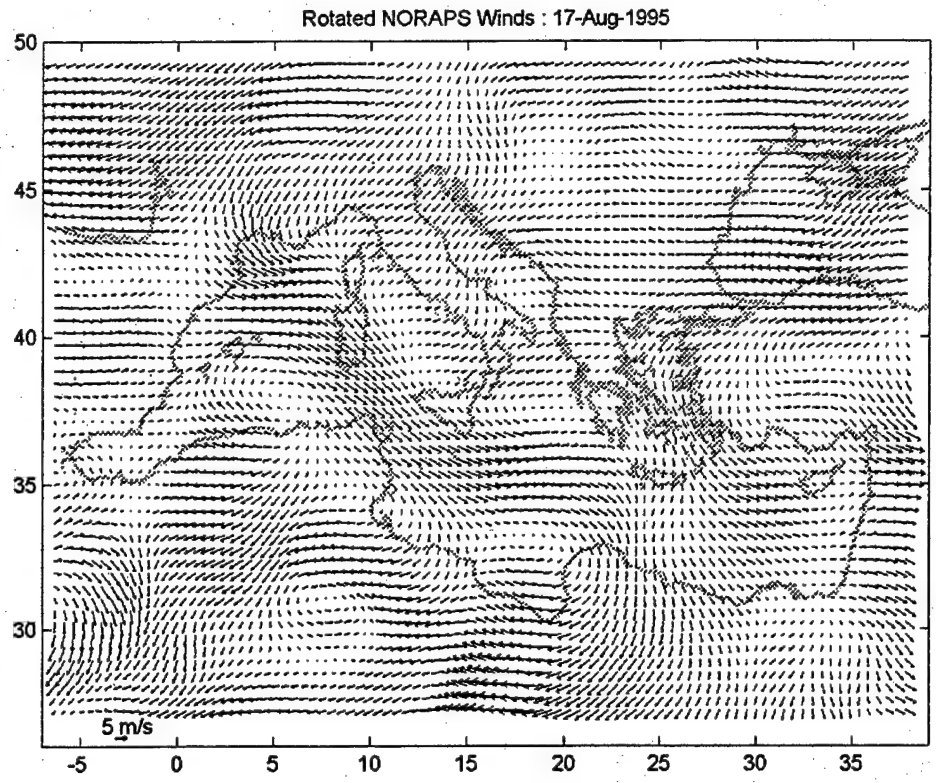

Figure III-4. Orographically steered NORAPS wind vectors for 17 August 1995.

B. METHODS

In order to use the satellite AVHRR data, it is essential to increase the accuracy of the sea surface temperatures, by using direct comparison with in situ (drifter) temperature data. Assuming that the drifter temperature data is "ground-truth," we can evaluate the accuracy of AVHRR data and make appropriate corrections by applying a bias offset to the entire AVHRR data set.

1. Calibration

In order to determine the accuracy of the AVHRR data set, it is first necessary to examine the availability of AVHRR data for a given day. This is a factor of three elements: 1) number of satellite passes over the area of interest every day, 2) percentage of good pixels available from a given satellite pass, and 3) availability of drifter temperature data for the area of interest. Figure III-5 shows a histogram of the number of satellite images for the time period between May 9 and October 21, 1995.

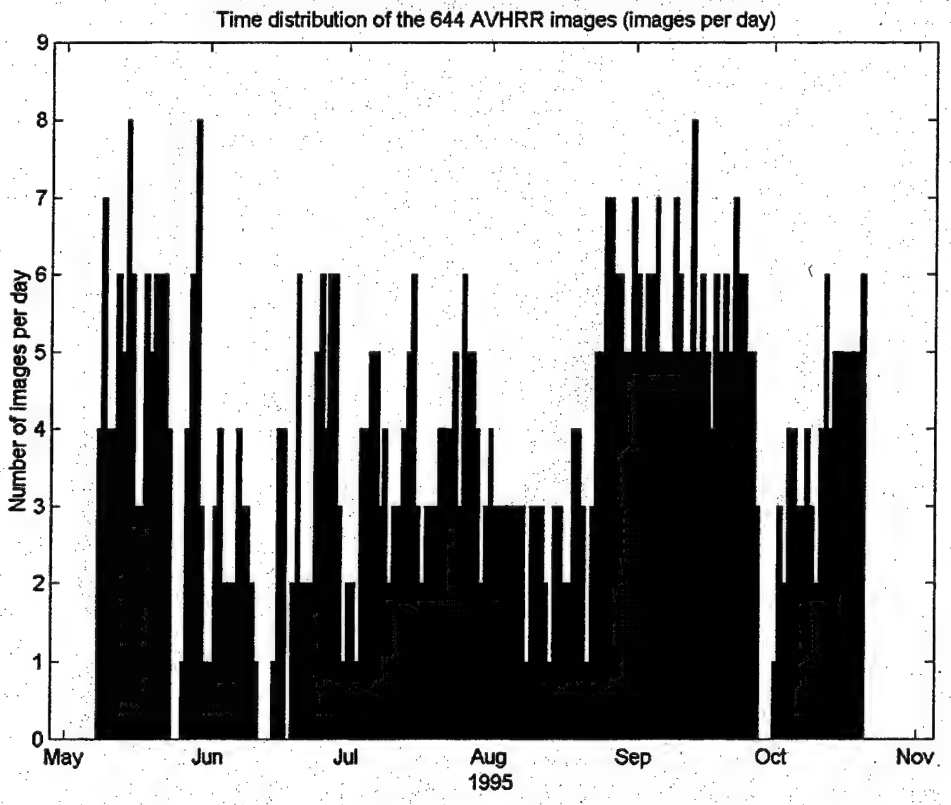

Figure III-5. Histogram of number of images per day from May to October, 1995.

Figure III-6 shows the percentage of masked pixels for each of the 644 AVHRR images.

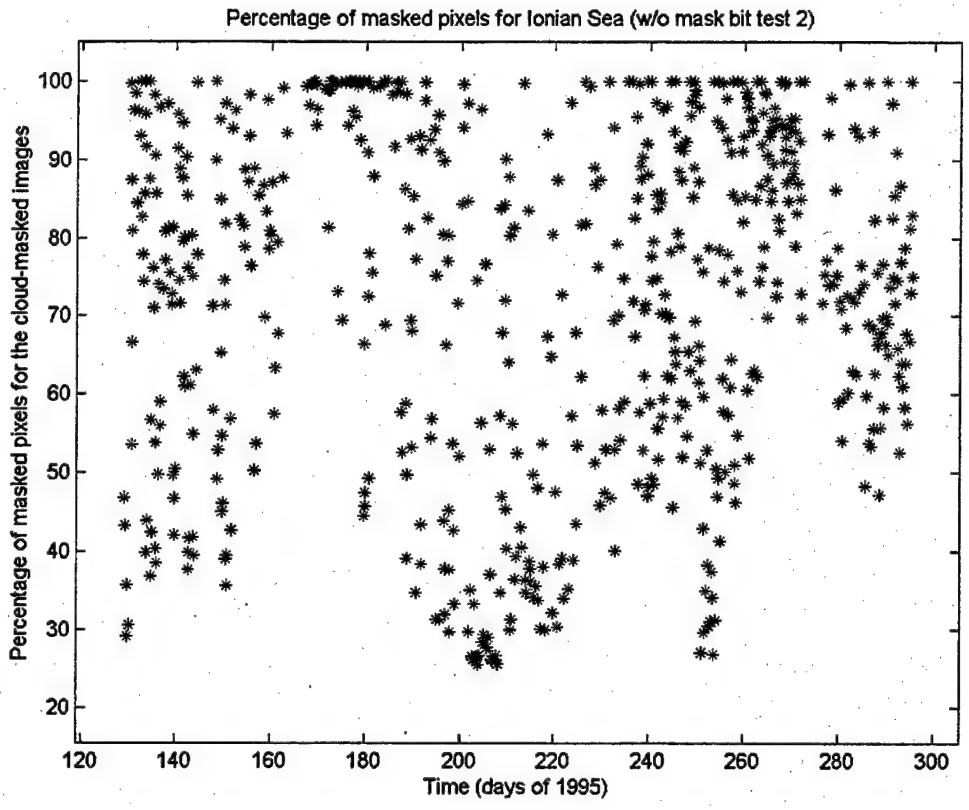

Figure III-6. Percentage of masked pixels per image for the Ionian Sea, for the time period May-October, 1995.

Here, 100 percent means that the entire image was masked, while the low number (25%) indicates an image on a clear day with only the land mask applied. A greater number of satellite passes per day, combined with a low percentage of

masked pixels per image, increases the likelihood that a pair of satellite and drifter temperatures can be compared. Drifter data were examined, and interpolated for data points that were missing sea surface temperature, latitude or longitude information. Satellite images and drifter data were examined for the combined Adriatic and Ionian Seas in order to maximize the SST range by including more spatial variability and hence increase the robustness of the bias constants. Every satellite image was masked (bit tests 1,3,4,5,6 and 7), and then compared with drifter data to find a match within a 15 minute window of the satellite image. Figure III-7 summarizes the location of all the pairs used for the drifter-satellite temperature pair comparison. The satellite image pixels and corresponding drifter data points were then grouped according to satellite MCSST algorithm (all NOAA-9 images, NOAA-12 day images, NOAA-12 night images, NOAA-14 day images and NOAA-14 night images). Each data set was finally processed to remove data point pairs for which the temperature difference departs by more than two standard deviations from the mean temperature offset. They were then analyzed using linear regression techniques. The results are summarized in Table 3.

Linear regression results are also graphed in Figures III-8 to III-12. In Figure III-8, the general trend has NOAA-9 under-estimate the sea surface temperature by a mean

value of approximately 0.91 °C. This mean temperature difference is the bias that was applied to all NOAA-9 AVHRR images. Likewise, in Figures III-9 to III-12, the NOAA satellites over-estimate the sea surface temperature by as much as 1.14 °C. In all cases, the mean temperature difference was applied to the respective AVHRR satellite images as a corrective bias.

satellite	time	Number of points	Correlation coefficient	Slope	Offset (°C)	Mean difference ($SST_{SAT} - SST_{DRIFTER}$) (°C)
NOAA-9	all	127	0.9755	0.9310	0.6403	-0.9100
NOAA-12	day	461	0.9873	0.9814	1.0414	0.6300
	night	946	0.9818	0.9986	0.3480	0.3300
NOAA-14	day	676	0.9861	1.0909	-0.9750	1.1400
	night	970	0.9860	1.0992	-1.5955	0.8400

Table 3. Linear regression results for Adriatic and Ionian Seas for the five MCSST algorithms.

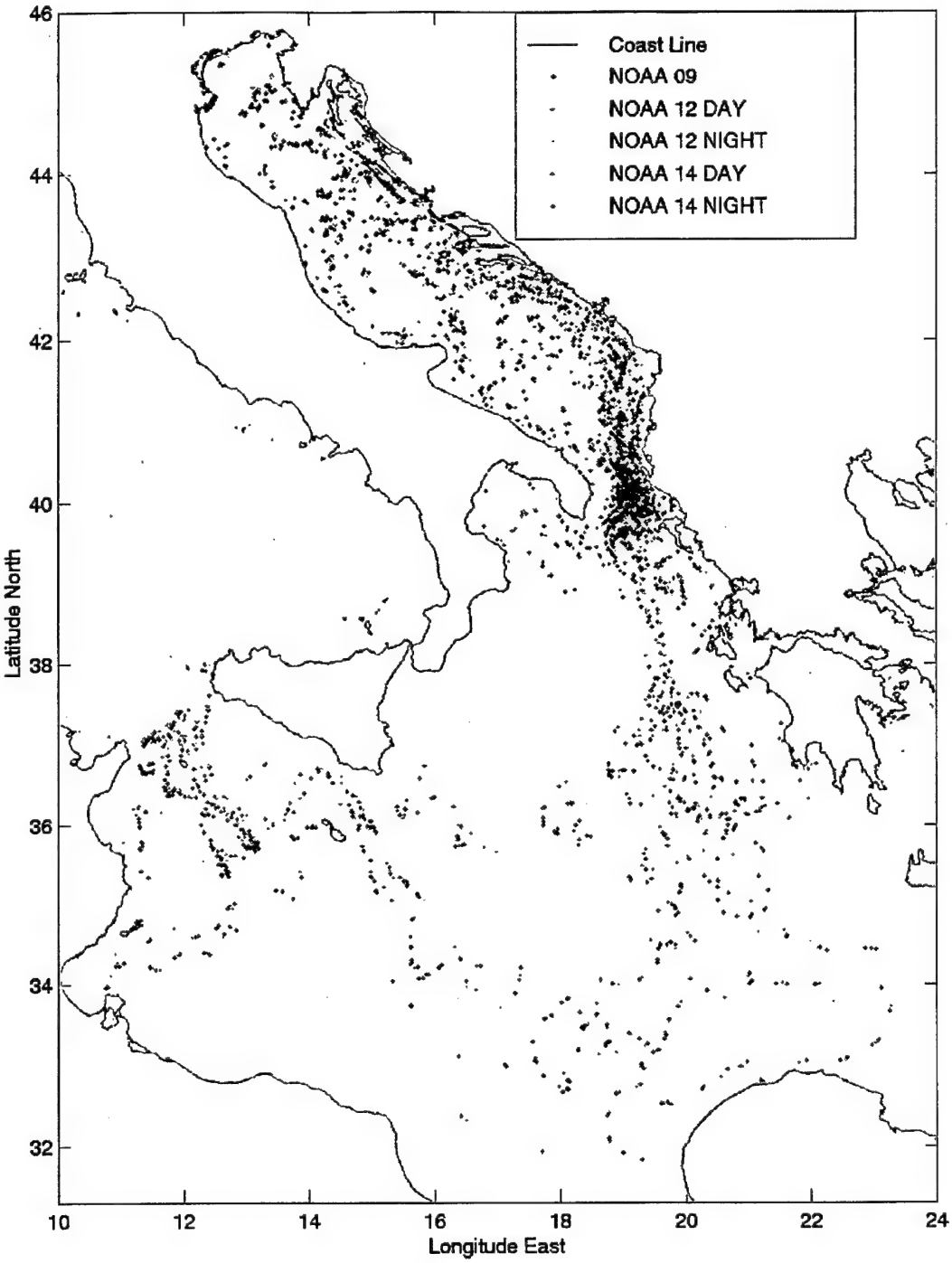

Figure III-7. Plot of the collocated and cotemporal satellite and drifter SST pairs, from 9 May to 22 October, 1995, considered to estimate SST bias offsets.

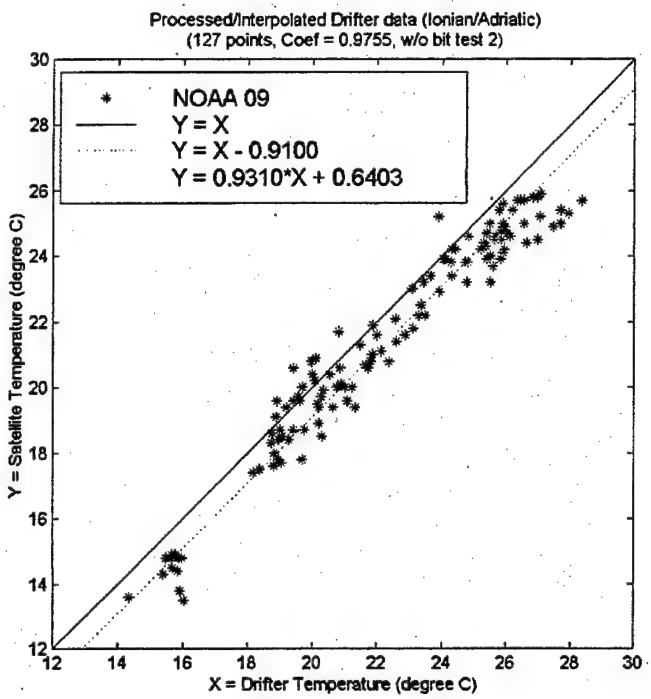

Figure III-8. Linear regression curves for NOAA-9 AVHRR data vs. drifter data.

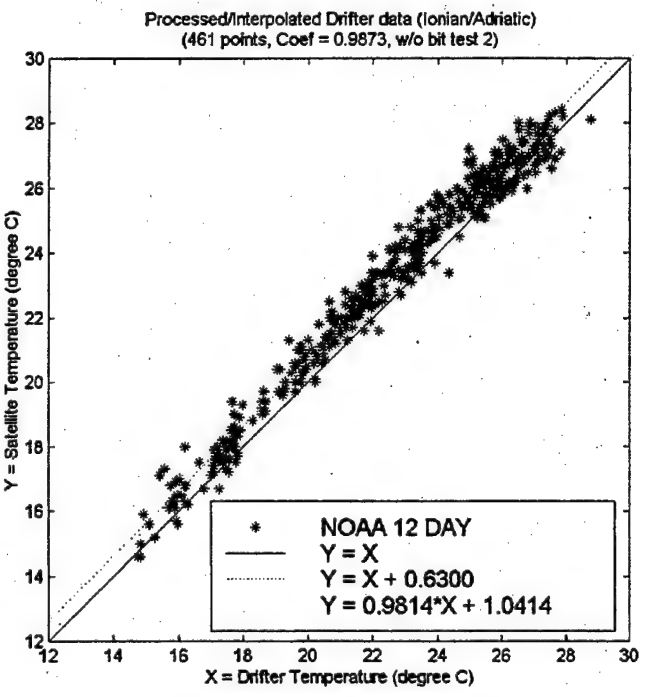

Figure III-9. Linear regression curves for NOAA-12 day AVHRR data vs. drifter data.

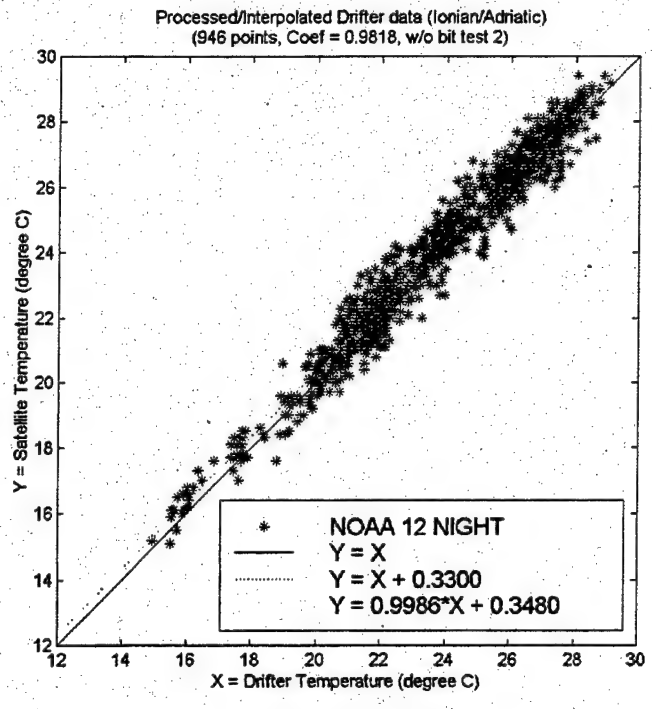

Figure III-10. Linear regression curves for NOAA-12 night AVHRR data vs. drifter data.

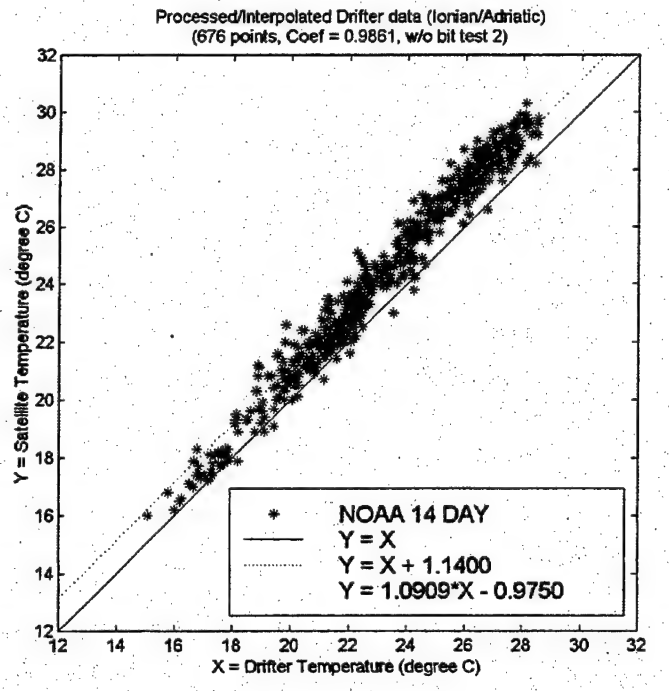

Figure III-11. Linear regression curves for NOAA-14 day AVHRR data vs. drifter data.

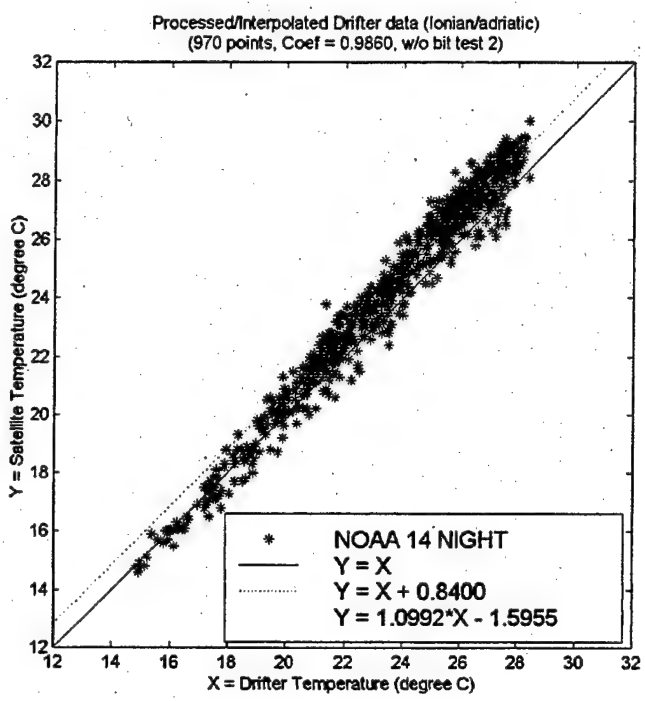

Figure III-12. Linear regression curves for NOAA-14 night AVHRR data vs. drifter data.

2. Climatology

Climatology is important in determining sea surface temperatures that are reasonable based on historical data for a specific region. Responsible for applying climatology to the satellite image mask, bit test 2 was determined to be too restrictive in eliminating AVHRR pixels, and therefore was not used in the image masking process. The climatology used in this study was interpolated from drifter data of the same time period, May to October 1995. Satellite pixel

temperatures were masked if not between the minimum and maximum drifter climatology values (Figure III-13).

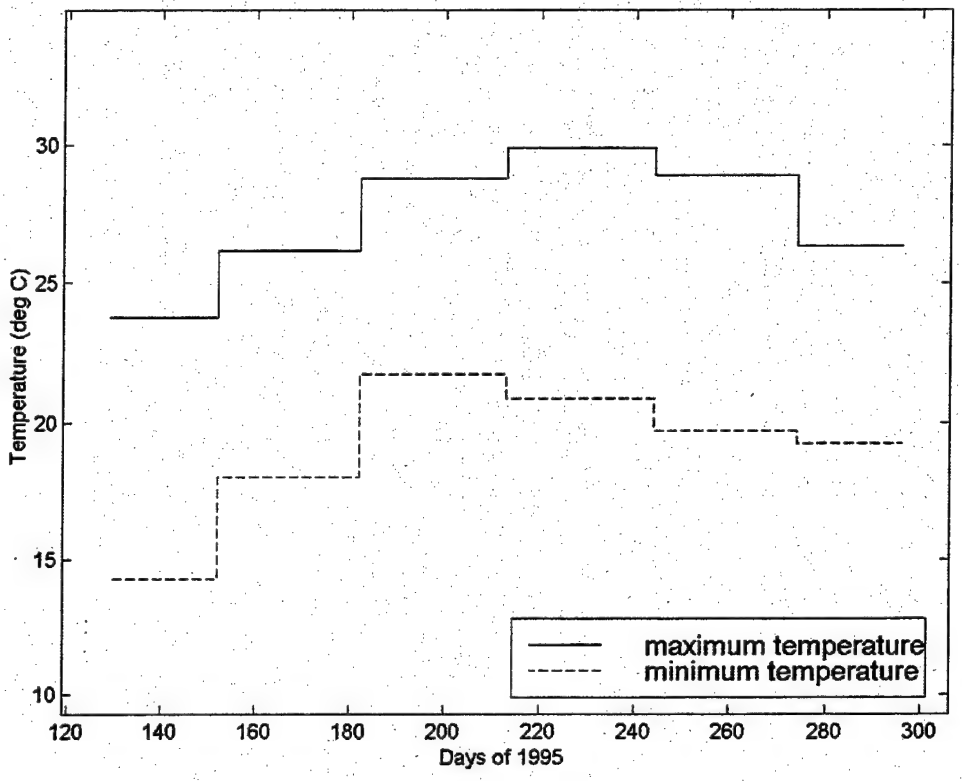

Figure III-13. Climatology temperature extrema estimated from the drifter data in the Adriatic and Ionian Seas during the period May-October, 1995.

3. Corrections

Before the AVHRR images could be used for statistical analysis, they were individually corrected for satellite bias and climatology. Using the results of linear regression analysis discussed above, the mean temperature difference was either subtracted or added to the entire satellite data set for each individual satellite image. The

above drifter climatology was applied to the images by masking the pixels with SST's outside the climatology range.

4. Diurnal Cycles

On specific days (especially during a calm summer day) a significant diurnal SST cycle can occur, with the possible maximum amplitude of 2° C (see Figure III-14). This can greatly affect the compositing process depending on the time of day from which the AVHRR data come. If an AVHRR image comes from an early part of the day, when the sun's heating effects are at a minimum, the composited image will underestimate the overall median SST. Likewise an image from the peak of the diurnal cycle will cause an overestimation of the composite's median SST.

In situ drifter data were analyzed to determine daily diurnal cycles as a possible bias correction to be applied to corresponding AVHRR images. Unfortunately, it was not possible to determine a satisfactory daily diurnal cycle for most of the days in the period of analysis because of the limited data available. The drifter SST's did not help because they were located in limited areas of the Adriatic and Ionian Seas. For example, drifters released in the Straits of Sicily were typically advected into the AIS and therefore recorded SST significantly lower than the mean

Ionian Sea SST. This localization bias could be corrected if SST data points could be collected from an evenly distributed locations throughout the Ionian Sea over a variety of times throughout the 24-hour period.

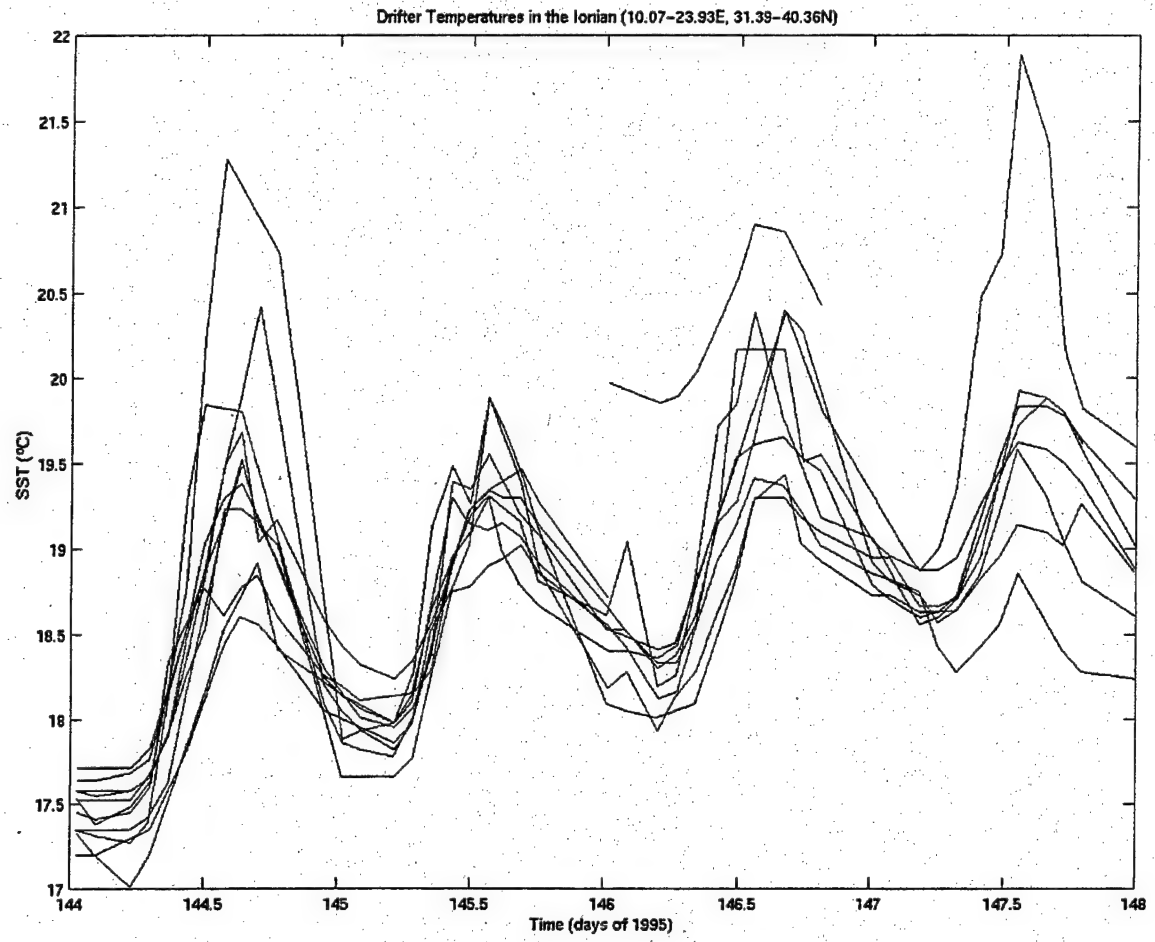

Figure III-14. Plot of drifter temperature data for period 24-26 May 1995 (days 144-147 of 1995). A significant diurnal cycle is evident over the four days, with typical amplitude of 1-2 °C.

5. Compositing

a) One and Three Day Composites

A composite image is generated by reading and processing each satellite image corresponding to the specified time period. Processing the image involves the application of a bias correction and climatology mask, as described previously. These images are then placed in a three dimensional array, hereafter referred to as the "cube". The cube is measured as an 800 by 1000 pixel array with a depth corresponding to the number of images in the specified time period for compositing. Statistics were used to determine the mean, median and standard deviation of sea surface temperature of each pixel of the 800x1000 array. In addition, the number of images used for compositing was determined and displayed for each pixel. The number of clear images per pixels is very important for a robust and accurate composite. Figure III-15 displays the percentage of clear images per pixel from 9 May to 22 October 1995. The distribution in the Ionian Sea is clearly zonal, with a higher percentage of clear pixels, or cloud free days, in the northern region. In the southern Ionian Sea and east of the Tunisian coast, the percentage of clear images drops to values near 30%. In general we can say that for most pixels, only a third of the raw images available have passed

the contamination tests and are therefore useful for subsequent analysis.

Figures III-16 and III-17 show the results for day 208 (27 July) of 1995. Figure III-16 uses bit tests 1, 3, 4, 5, 6, and 7, while Figure III-17 uses only the land mask (bit test 6) to eliminate contaminated pixels. Here, composite images of the mean SST, median SST, SST standard deviation, and number of images per pixel are displayed. Of particular note, is the presence of a sharp temperature change in the mean SST composite (Figures III-16a and III-17a) running north-south through the center of the Ionian Sea. This irregularity is not as distinguishable in the median SST composite (Figures III-16b and III-17b), however is clearly visible in the SST standard deviation (Figures III-16c and III-17c) and the number of images per pixels (Figures III-16d and III-17d). The banded structure of these images, with sharp discontinuities separating regions with three, four, five and six pixels is due to the different swaths of the satellite passes. The effect of these discontinuities appears less evident in the median SST map compared to the mean SST map.

In Figure III-18, the mean SST, median SST, SST standard deviation, and number of images per pixel are displayed for a three-day composite centered around 12 July, 1995. This is a worst-case scenario, where very few images

(Figure III-18d) are available for the three day time period. Off southwestern Greece and the eastern Tunisian coasts, a few areas of six images per pixel can be noted; however, the overall image pixel count is much lower, approximately two to three images per pixel. There are even some areas where no images were available, most notably southeast of Sicily. The effect of the low number of image pixels can be clearly seen in the mean SST (Figure III-18a), median SST (Figure III-18b), and SST standard deviation (Figure III-18c) maps. Where no images were available for comparison, no SST can be computed, thus the data absence is denoted by a blackened area in the mean and median SST composites. In addition, where there is one or no image available, no SST standard deviation can be computed and is represented by zero, or blackened areas (Figure III-18c). Sharp temperature gradients can be seen in the southern Ionian Sea in Figures III-19a, b, c. As in Figures III-16 and III-17, they clearly correspond to areas where image count per pixel rapidly changes, resulting in uneven compositing smoothness. This contrasts significantly with the next three-day composite for July 14-16, 1995 (Figure III-19). The mean and median SST composites of Figure III-19 show a generally smoother SST distribution than in Figure III-18. The number of images per pixel is much higher, with the northern Ionian Sea well above nine images per pixel.

This produces more realistic mean and median SST composites, displaying the characteristics of large sea surface structures, such as cold water upwelling off the western tip of Sicily or the large warm patches of surface water in the interior of the Ionian Sea. Some of the true temperature structures apparent in Figure III-19 (southwestern Ionian) have been smoothed out in Figure III-20, due to their variability over the seven-day period.

b) Weekly and Monthly Composites

The weekly and monthly composites were assembled as described above, except over a longer period. Figure III-20 shows the week of July 11-17, 1995. As a combination of Figure III-18, Figure III-19, and images for July 17, 1995, Figure III-20 shows in general more smoothness of temperature signatures with respect to the three-day mean SST composites. However, the median SST composite still shows distinct mesoscale and sub-basin, such as upwelling off the Sicily and Greek coasts.

Figures III-21 and III-22 display the results for July, 1995, using only the day and night images, respectively. The day and night July composites were generated to examine possible effects of diurnal heating in late afternoon images on calm days (Philippe and Harang,

1982). Looking at the mean SST (Figures III-21a and III-22a) and median SST (Figures III-21b and III-22b) composites, sub-basin features are clearly visible, such as upwelling off the Sicily coast, the current pattern of the AIS, the Cretan Cyclone, and the general warm water mass in the southern and central Ionian Sea, with little difference between day and night composites. The small difference between the day and night images permit the use of both kinds of images for all composites. The night images of July (Figure III-22) show some noticeable artificial gradient lines in Figure III-22a, c and d. As shown in Figure III-23, when the day and night composites of July are combined, there is little difference between the day/night July median and the July median SST composites. The large number of clear pixels (maximum of 74) smooth out any artificial discontinuities in the SST maps.

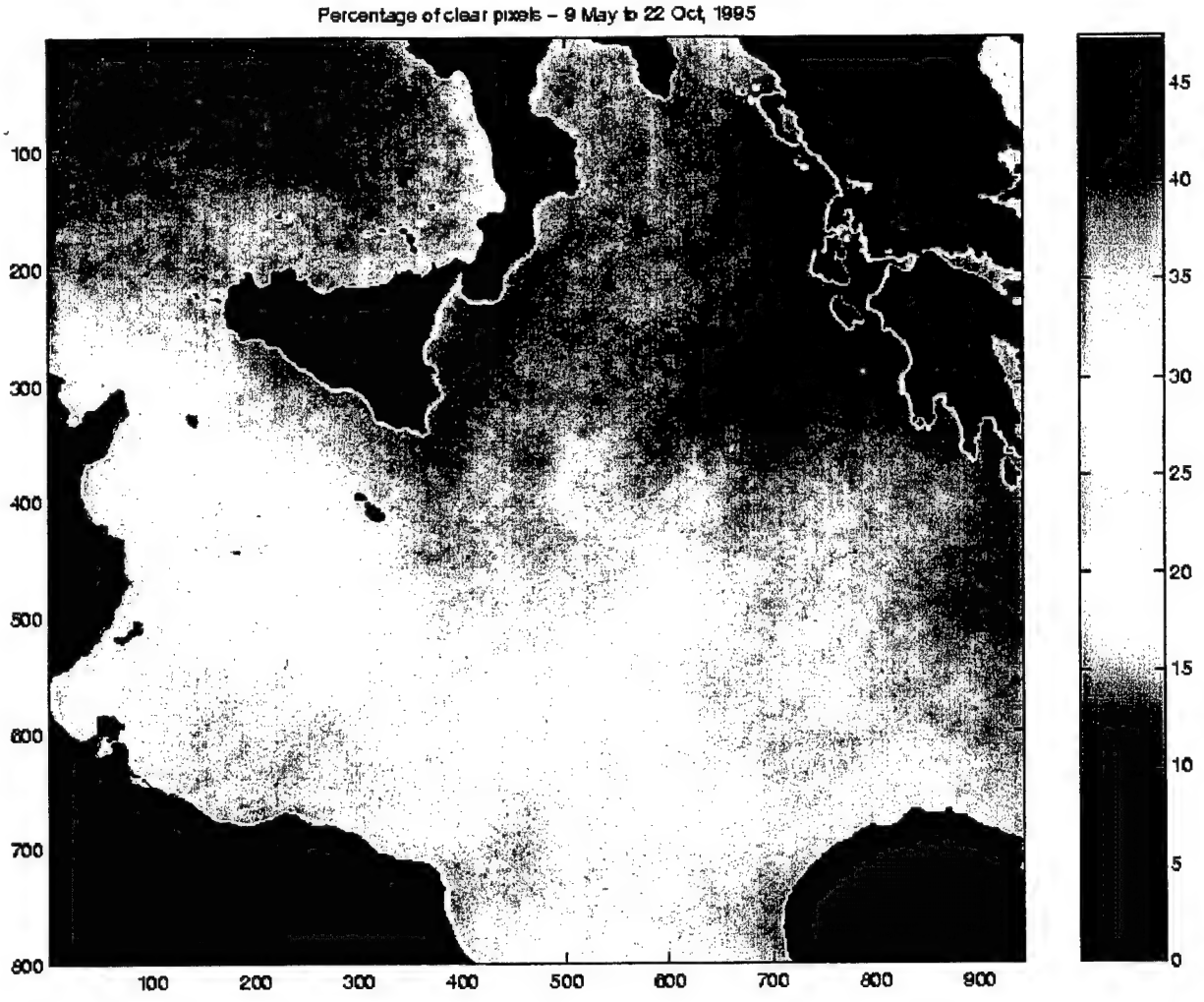

Figure III-15. Plot of percentage of clear pixels for the Ionian Sea for the time period between 9 May and 22 October 1995.

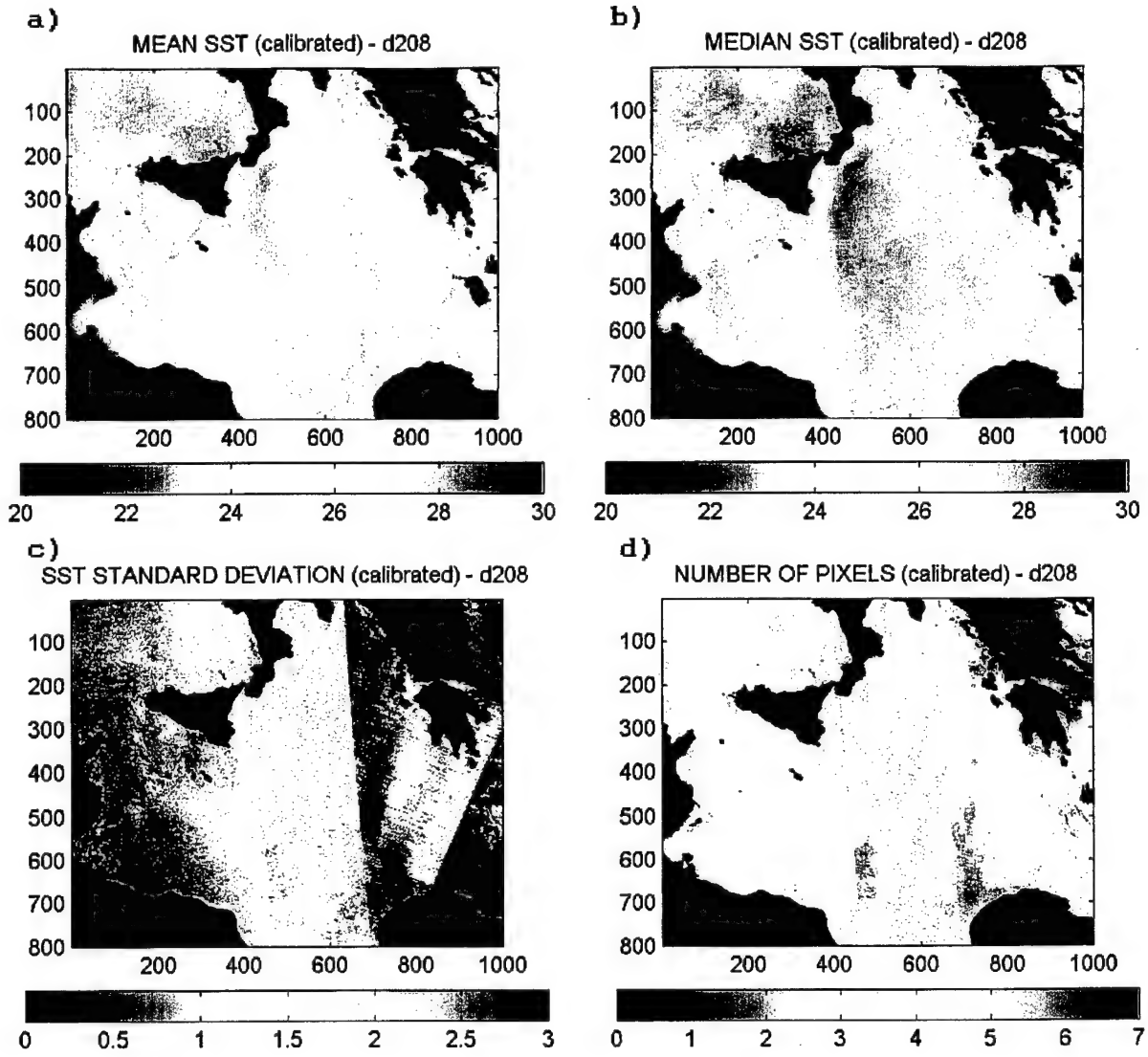

Figure III-16. Plot of composite image of (a) mean SST, (b) median SST, (c) SST standard deviation, and (d) number of pixels for day 208 (27 July 1995), with all mask tests (1, 3, 4, 5, 6 and 7) applied.

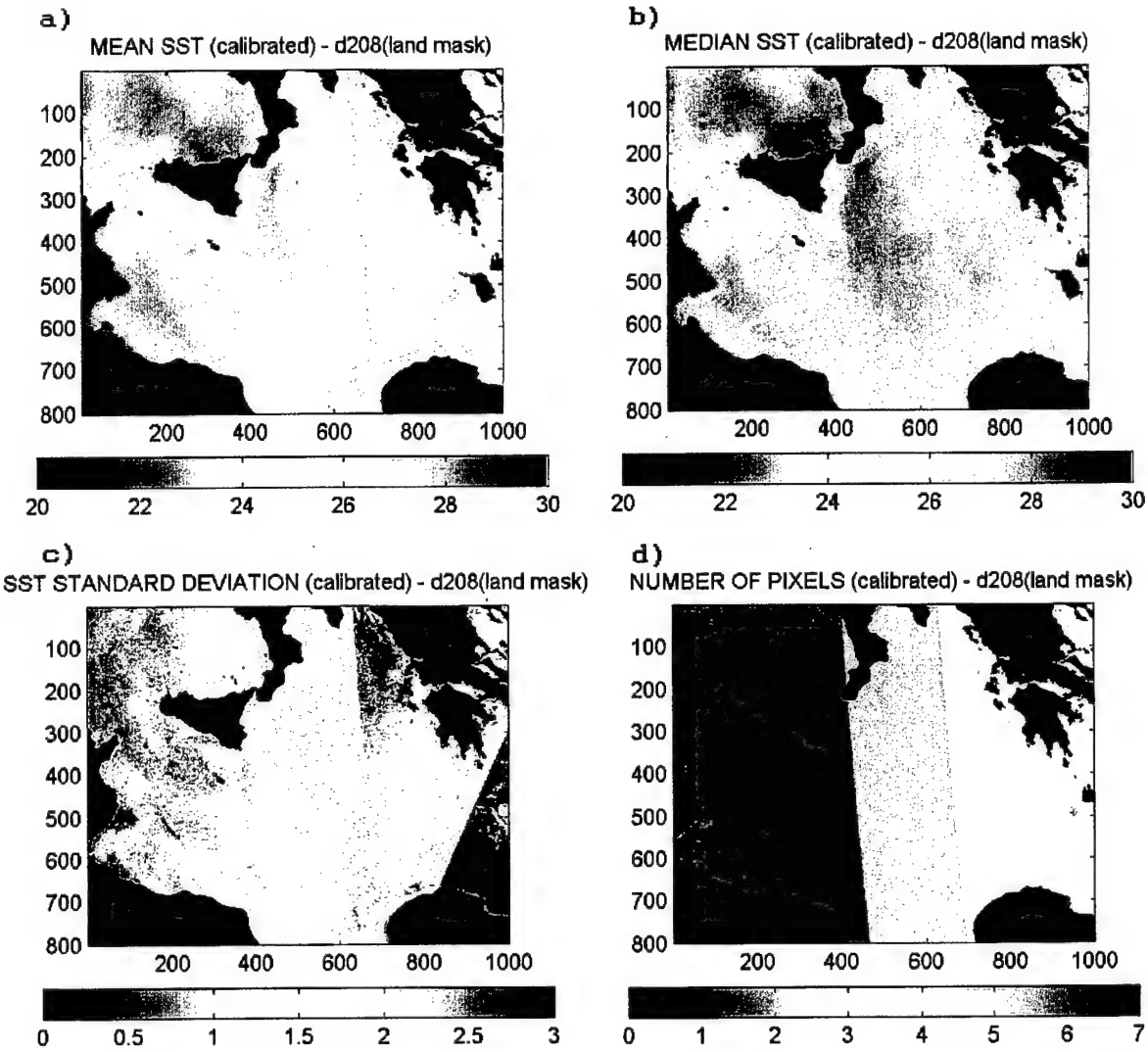

Figure III-17. Plot of composite image of (a) mean SST, (b) median SST, (c) SST standard deviation, and (d) number of pixels for day 208 (27 July 1995), with only land (test 6) mask applied.

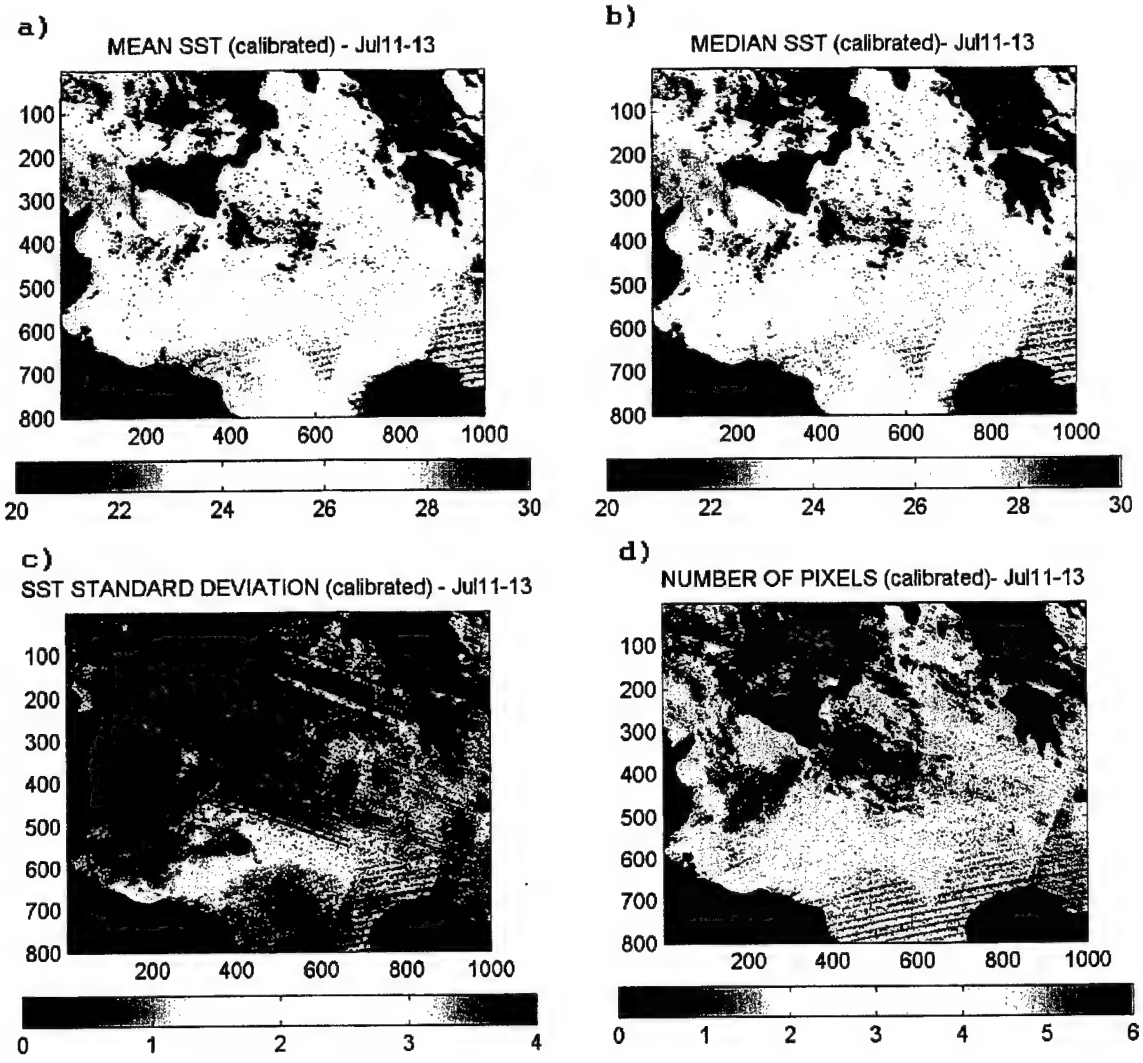

Figure III-18. Plot of composite image of (a) mean SST, (b) median SST, (c) standard deviation SST, and (d) number of pixels for July 11-13, 1995.

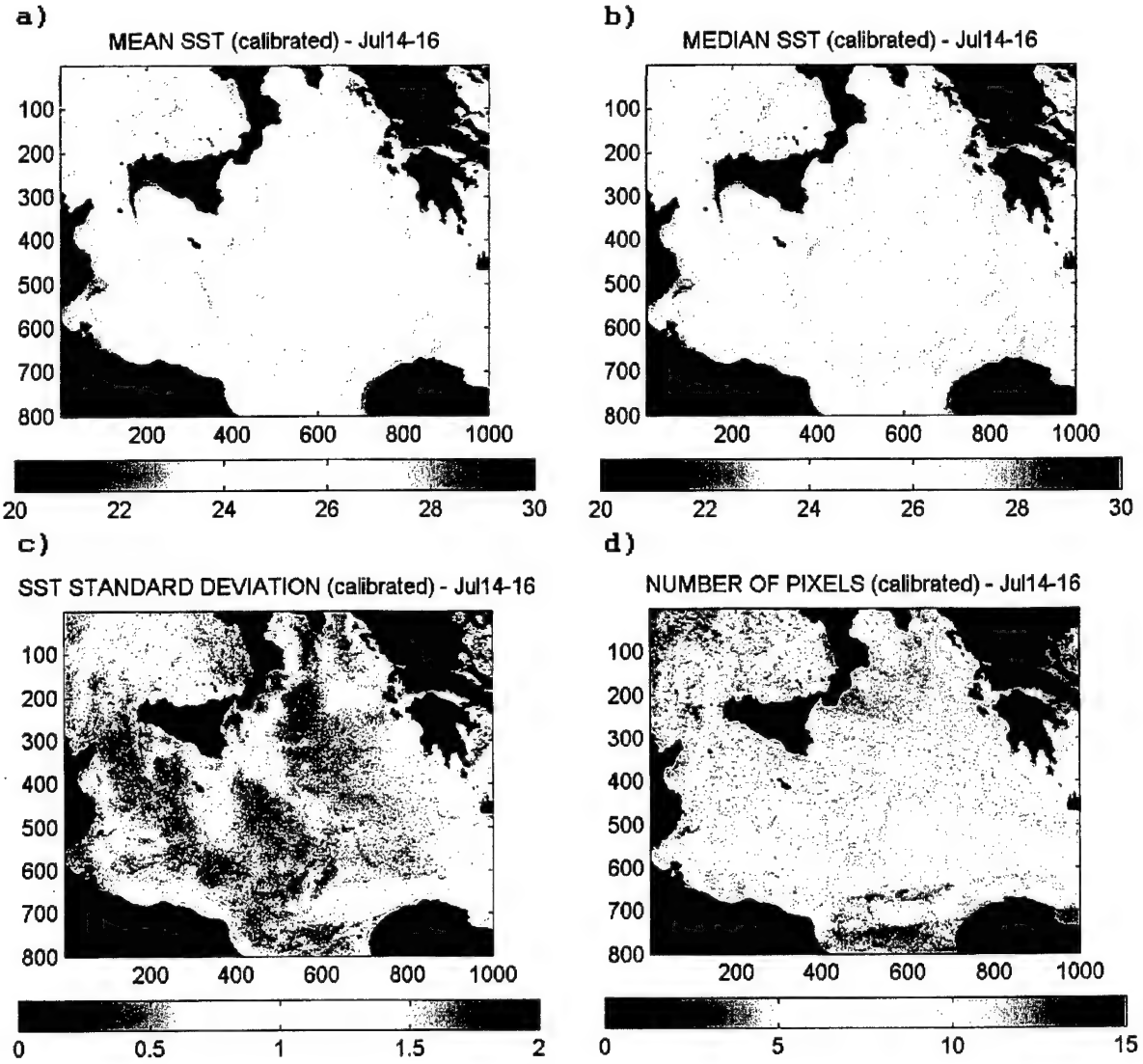

Figure III-19. Plot of composite image of (a) mean SST, (b) median SST, (c) standard deviation SST, and (d) number of pixels for July 14-16, 1995.

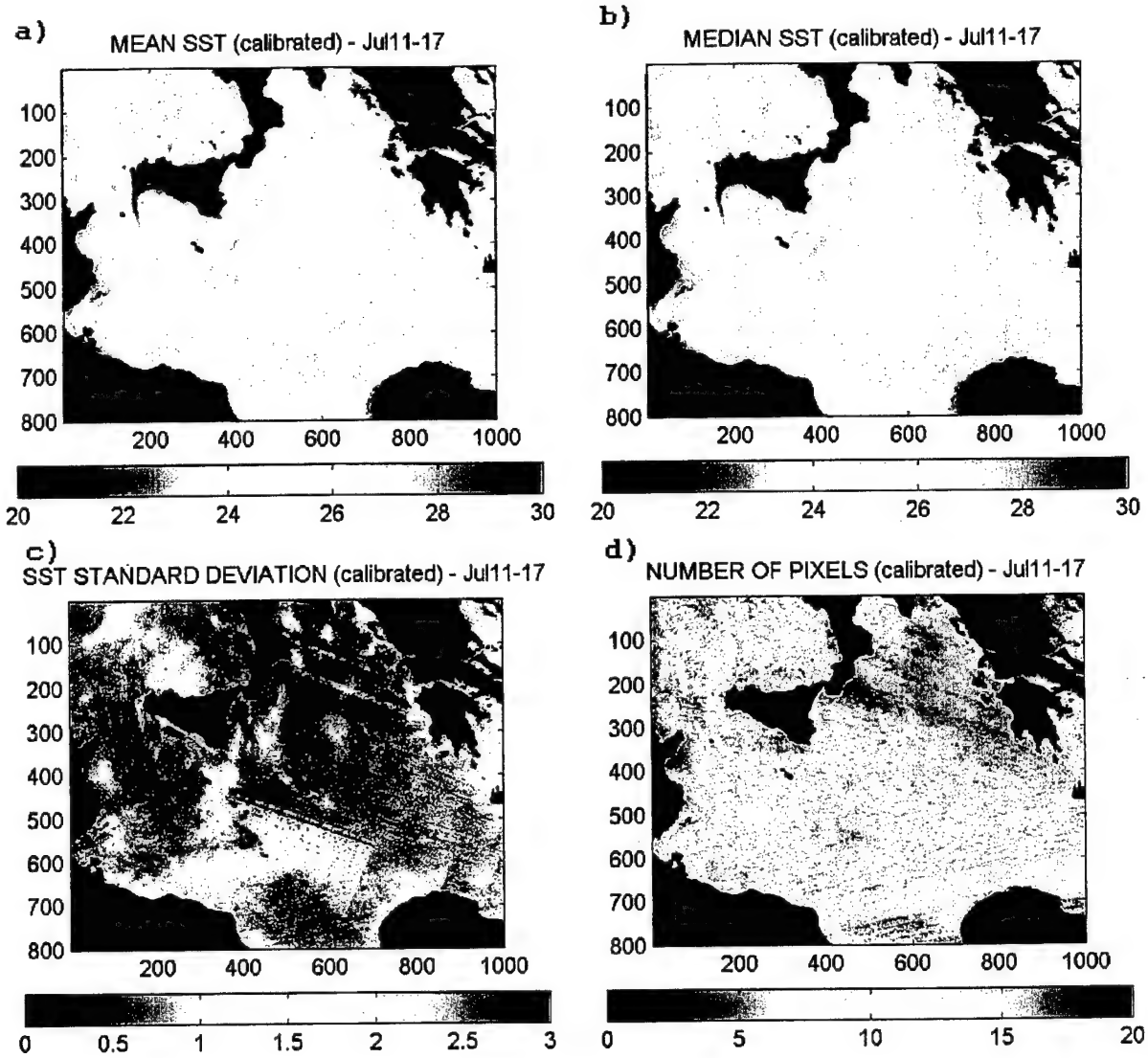

Figure III-20. Plot of composite image of (a) mean SST, (b) median SST, (c) standard deviation SST, and (d) number of pixels for July 11-17, 1995.

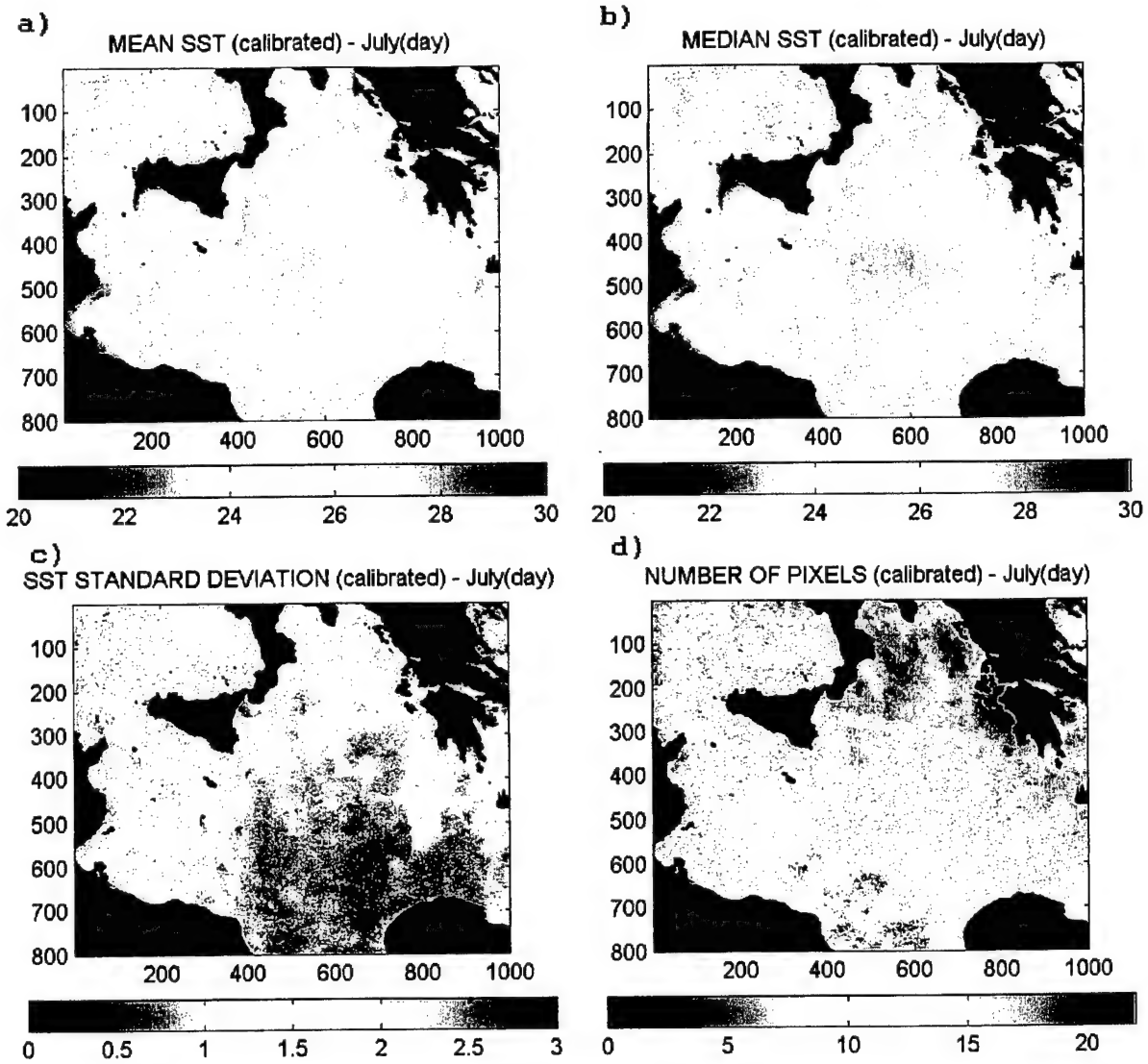

Figure III-21. Plot of composite image of (a) mean SST, (b) median SST, (c) standard deviation SST, and (d) number of pixels for July, 1995 (daytime only).

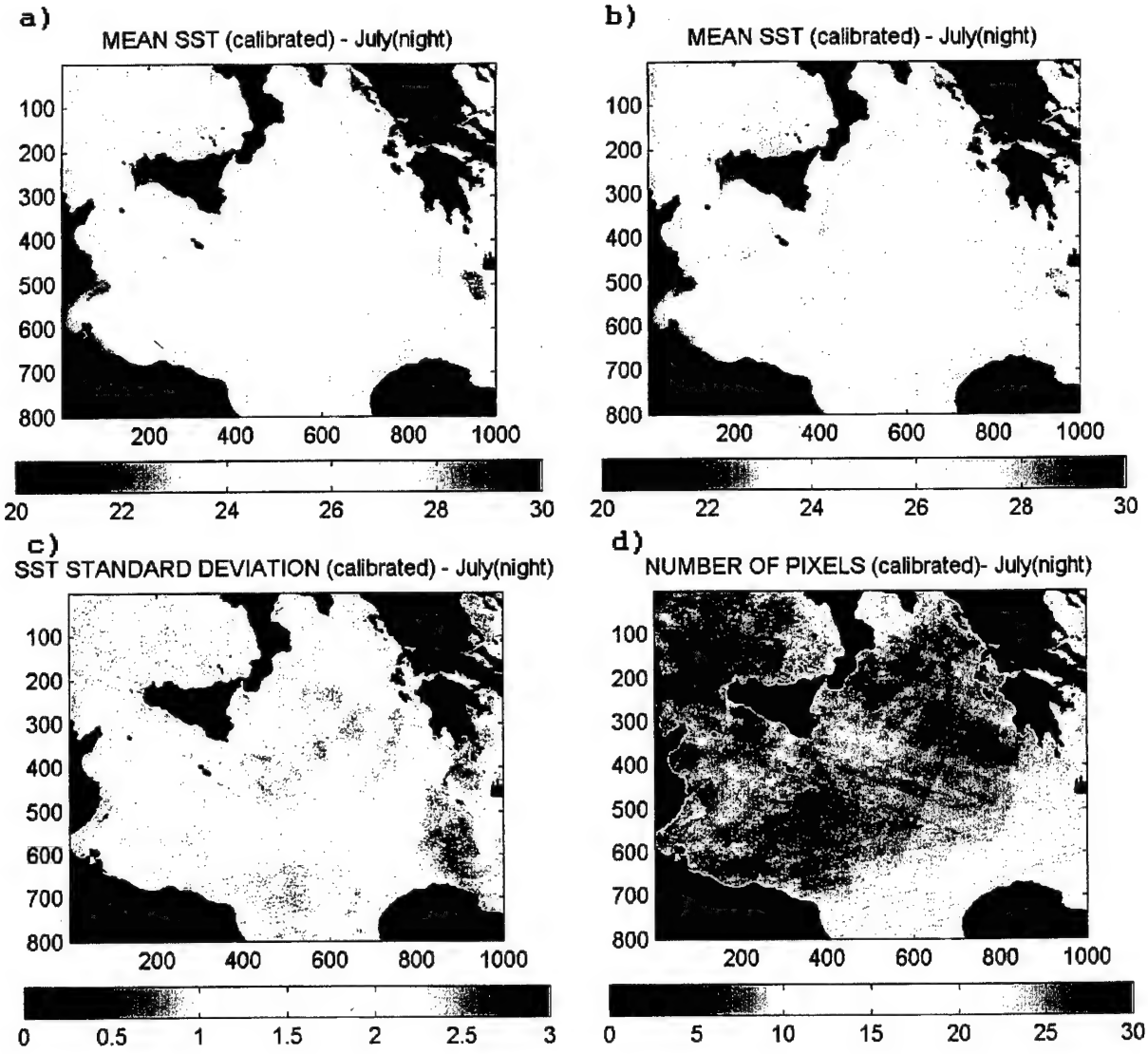

Figure III-22. Plot of composite image of (a) mean SST, (b) median SST, (c) standard deviation SST, and (d) number of pixels for July, 1995 (nighttime only).

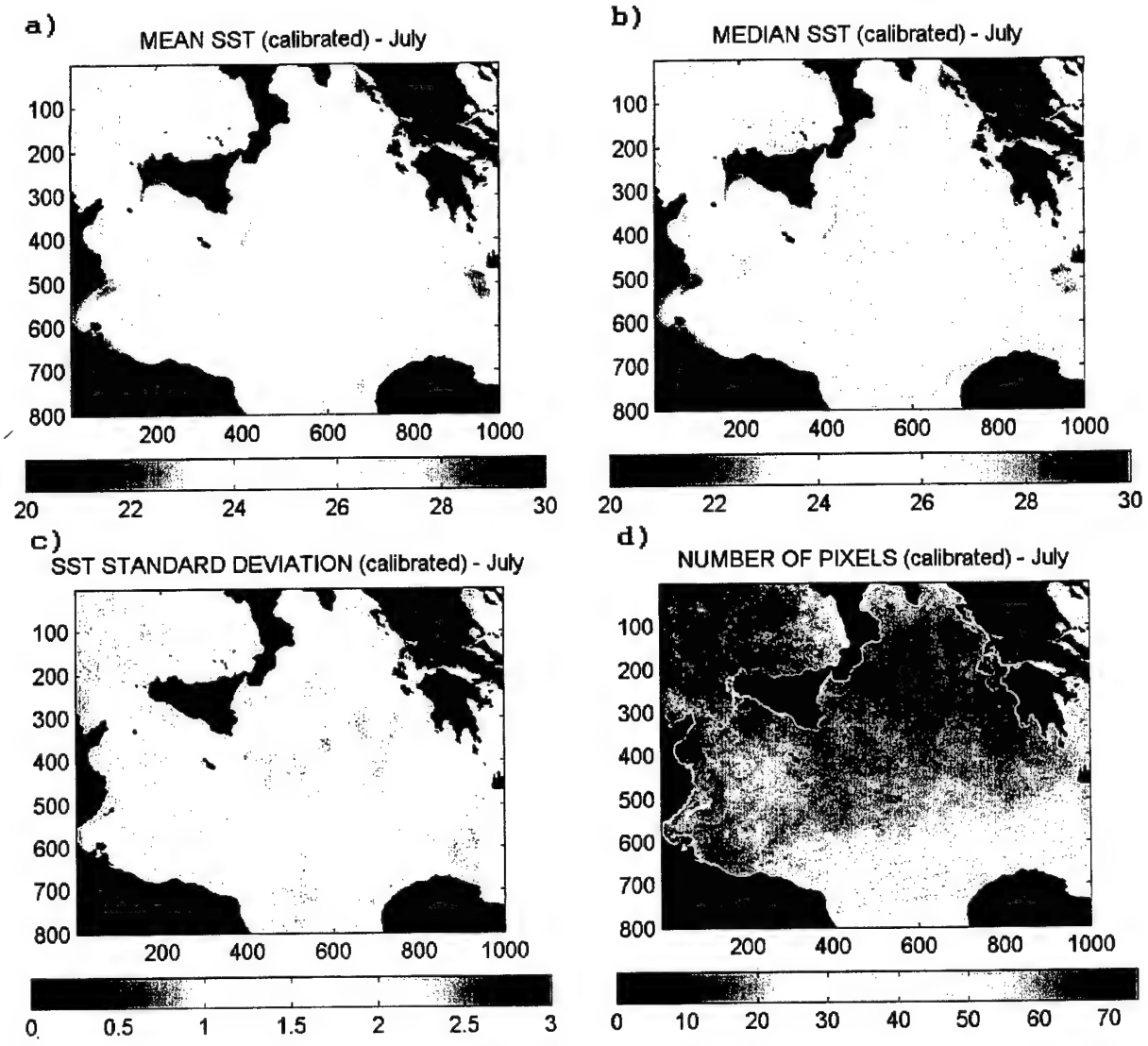

Figure III-23. Plot of composite image of (a) mean SST, (b) median SST, (c) standard deviation SST, and (d) number of pixels for July, 1995.

IV. RESULTS

The compositing techniques detailed in Chapter III were used to create composites for daily, three-day, weekly, and monthly time periods.

A. MONTHLY COMPOSITES

The time period from May to October, 1995 covers a wide range of seasonal variability of the Ionian Sea. May and June is characterized by a transitory period from winter to summer. July, August and September includes a strong summer meridional SST distribution. October begins to show the annual seasonal change with a gradual cooling. Figure IV-1 shows the spatial mean of the weekly median sea surface temperature composites for the Ionian Sea. In addition, the maxima/minima temperature drifter climatology (from Figure IV-13) and SST standard deviation are plotted. The median temperature shows a wide range of temperatures. From a summer maximum of 27.4 °C in August to a minimum of 17.4 °C in May, the Ionian Sea displays significant seasonal sea surface temperature variability. It can also be seen that the climatology derived from the drifter data contains the mean of the weekly median temperature composites, as expected.

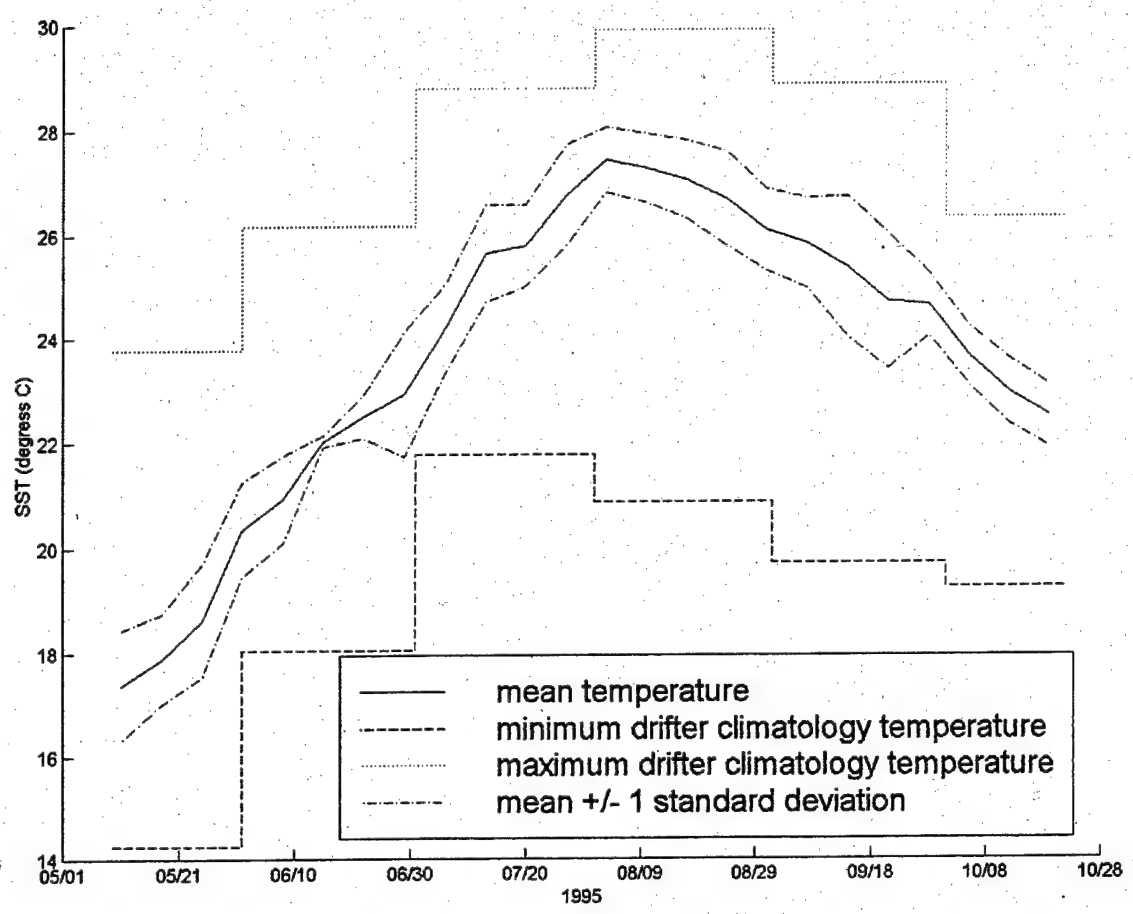

Figure IV-1. Plot of the spatial mean of weekly median temperature composites for the period from May to October, 1995. The SST climatology range obtained from the drifters are also shown.

The May composite (Figure IV-2a) shows the overall cool sea surface temperature of the Ionian Sea, with the expected warmer waters off the northern coast of Africa. The AIS can be faintly discerned entering the Straits of Sicily, moving northeast towards the Adriatic Sea, but then disappears into the background. Some upwelling signature is also evident along the southern coast of Sicily. Very

cool waters are flowing out of the Adriatic Sea through the western side of the Strait of Otranto. The June composite (Figure IV-2b) is characterized by a general warming trend in the Ionian Sea, however there is little evidence of typical Eastern Mediterranean Sea features. This is due to the lowest number of satellite images available (Figure III-5) for compositing, and a result of the high number of contaminated pixels (Figure III-6).

In July (Figure IV-3a) the warming trend of the Ionian Sea continues. The upwelling off the western tip of Sicily is highly visible, as is the Cretan Cyclone, with its cold water off the southwestern coast of Crete, and finally, upwelling is apparent on the eastern side of the Strait of Otranto. In August (Figure IV-3b), the Ionian Sea's surface temperature increases by a few more degrees. The cold water associated with the upwelling off the Sicily coast expands offshore. The Cretan Cyclone is still apparent, though cooler water from the Aegean Sea appears to be flowing into the eastern side of the Ionian Sea.

The AIS appears to have the strongest temperature signature in the September composite (Figure IV-4a). The AIS and its extension into the northern Ionian can be discerned reaching the region south of the Strait of Otranto, before turning southeastward towards the Cretan

Passage. There is also a distinct north-south separation of water, with the cooling northern Ionian and still warm southern Ionian. The Cretan Cyclone is weak. The October composite (Figure IV-4b) shows continuing cooling of the Ionian Sea. The MMJ can be seen as a cold current flowing from the western Greek coast towards the northern African coast off Libya. The Cretan Cyclone has the strongest temperature signature.

B. WEEKLY COMPOSITES

Figure IV-5 shows the median sea surface temperature anomaly for the week of August 29 to September 4, 1995. A spatial mean of 26.14 was removed to define the SST anomaly. The weekly mean rotated NORAPS winds are overlaid as blue arrows, showing the surface wind direction and strength. In addition, co-temporal drifter positions are plotted (stars and circles corresponding to start and ending positions, respectively) for a ten-day period, extending 1.5 days before and after the weekly period of the composite image. The plots of ten-day drifter trajectories allow easier tracking of specific drifters over successive weekly composites. Here, strong northwestern Mistral winds can be seen over the Strait of Sicily. Combined with the orientation of the southwestern

coast of Sicily, the mistrals cause significant coastal upwelling. It can be seen that the surface currents flow faster under the influence of the AIS and the MMJ, as disclosed by the longer drifter tracks in the cooler waters of the AIS/MMJ versus the shorter drifter tracks over the Tunisian Shelf. Traces of the MMJ off the Greek coast are evident in the south southeastward direction of the nearby drifter tracks, while there is a faint sea surface temperature signature.

In contrast to the strong mistrals, a very different wind condition prevails just two weeks after (August 8-14, 1995; see weekly composite in Figure IV-6). Here the winds over the Ionian Sea are very weak in comparison with the previous figure, although they appear to have an anti-cyclonic rotation centered on the southern tip of Sicily. Noteworthy is the increase in the negative temperature signature of the Cretan Cyclone with the northerly Etesian winds blowing from the Aegean Sea. The westward veering of these winds in the southern Ionian cause significant upwelling off the African coast near Tripoli and Benghazi (see geographical locations in Figure IV-7). Since the winds have weakened and reversed in the Straits of Sicily, the upwelling off the Sicilian coast appears much reduced.

C. UPWELLING REGIONS

Several regions in the Ionian Sea were subject to events of upwelling during the period of analysis. Five areas were selected for the consistent appearance of upwelling events. Their locations are shown in Figure IV-7. For the five areas observed, events of upwelling of cold water from sub-surface sources are represented graphically (Figure IV-8) from May to October, 1995 as minima in sea surface temperature. These data points were obtained by averaging the masked temperatures in a 9x9-pixel area centered on the areas of interest for all available AVHRR images. Times with no available data in Figure IV-8 are due to the absence of clear pixels, as displayed in Figure IV-9. In addition, further analysis was done to compare wind speed with SST. To avoid contamination from mean SST's with a low number of non-contaminated pixels, a minimum threshold of 20 clear pixels was used for further plotting and for computing correlation coefficients (Figures IV-10 to IV-14).

Near Tripoli, there is a weak (0.009), but positive correlation between the northwesterly wind component and the SST off the coast (Figure IV-10). One of the strongest upwelling events occurs around day 223 (August 11, 1995) and is clearly visible in Figure IV-6. The Cretan Cyclone

is represented by area A2, off the western coast of Crete. Here the correlation coefficient is quite large (0.45), meaning that with winds from the north (Figure IV-11b) there is a decrease in sea surface temperature (Figure IV-11a). Two large upwelling events are observed around days 209 (July 28, 1995) and 226 (August 14, 1995), the latter corresponding to the large cold sea surface temperature anomaly shown in Figure IV-6. The cyclone's cold temperature is also recognizable in the monthly composites of July, August, September and October (Figures IV-3 and IV-4, respectively).

Off the coast of Benghazi (Figure IV-7), the correlation coefficient between the southwesterly wind component and SST (Figure IV-12a, b) is still positive (0.20). There is a major single event around day 225 represented in Figure IV-6 and which can even be discerned in the monthly composites of June, July and August (Figures IV-2b, IV-3a and b, respectively). In the eastern Strait of Otranto (area A4) there is a positive correlation (0.25) between the SST and the northerly winds (Figure IV-13). Cold water is mostly present throughout the period of study.

D. THREE-DAY COMPOSITES

Three-day composites were generated for the entire Ionian Sea, however the Straits of Sicily were of particular interest due to the temporal variability caused by the influences of the AIS and the upwelling events forced by the Mistral winds. As an area of upwelling, the region south of Sicily (area A5) has a negative correlation coefficient (-0.14, see Figure IV-14) meaning that positive winds blowing from the northwest correspond to cool waters. The effects of the Mistral winds are clearest in Figure IV-5, and the monthly signature of upwelling is present in all the monthly composites (Figures IV-2, 3 and 4).

Beginning on July 5, 1995 and ending on September 5, 1995, twenty-one three-day composites are presented in Figures IV-15 to IV-21, to better understand the characteristics of upwelling and the AIS in the Straits of Sicily. The first three composites (Figure IV-15) contain no drifter data, but show upwelled cold water that is entrained by the AIS away from the Sicily coast towards the Tunisian shelf, while another jet moves along the Sicily coast, forming the Maltese Channel Crest (MCC) (Robinson et al., 1999). The current then moves northeast of Malta, forming the Ionian Shelf Break Vortex (IBV) or Malta front (Briscoe et al., 1974) before continuing north (Robinson et

al., 1999). In addition, the cold water from the southwestern tip of Sicily flows to the south-southeast and forms the southern limb of a cyclonic circulation feature on the eastern edge of the Adventure Bank, named the Adventure Bank Vortex (ABV) by Robinson et al. (1999).

In the waters between Sicily and the Italian peninsula, the Strait of Messina is an area where tidal mixing (intermittent in late spring and early summer) of cool Atlantic and warm Levantine waters is strengthening (Bohm and Salusti, 1984). This phenomenon is responsible for the patch of cold water that occurs intermittently in July (principally during the period 5-7 July 1995, Figure IV-15a).

The next three composites (Figure IV-16) show a stronger upwelling sea surface temperature off the Sicily coast. A single drifter caught in the AIS moving south with the cool water. The third set of composites (Figure IV-17) shows the release of a number of drifters in the Straits of Sicily. The first half-loop (ABV) of the AIS is strong, as evidenced in the longer drifter tracks near the upwelling vice the short tracks off the Tunisian Shelf. The AIS can be seen to bifurcate west of Malta, as two drifter tracks part, one traveling north towards Sicily, and the other moving southwest towards the Tunisian Shelf

(Figure IV-17c). Also, the ABV can been seen as a weak temperature signature east of the AIS, continuing in Figure IV-18. Starting with August 1, 1995 (Figure IV-18) the drifter paths continue between Malta and Sicily, the second loop of the AIS near Sicily that forms the IBV. In addition, a number of drifters located on the Tunisian Shelf are advected into the AIS, and swiftly moved north. The drifters continue to follow the AIS, despite the reduced sea surface temperature signature of upwelling off the Sicily coast (Figure IV-19). In Figures IV-20 and 21, the upwelling sea surface temperature and ABV signature increases. The strongest anomaly appears during the period of August 28 to September 2. Some of the drifter tracks do not follow the path of the AIS; rather they move southeast off the Malta coast or continue south on the Tunisian Shelf.

Throughout Figures IV-15 to IV-20, the upwelling off the western tip of Sicily is evident as a filament of cold water moving towards the center of the Straits of Sicily. Coastal upwelling along the remainder of the southwestern coast of Sicily is also apparent. Of note is the enhanced negative temperature signature of the general coastal upwelling and the presence of a strong upwelling filament off the western tip of Sicily typically associated with

strong Mistral winds for the time period of 5-24 July 1995 (Figures IV-15a to IV-17a). From 25 July to 14 August 1995 (Figures IV-17a to IV-19c), Mistral winds are replaced by a constantly shifting wind pattern resulting in weakened upwelling along the southwestern coast of Sicily. Finally, the Mistral winds return to the Straits of Sicily, causing increasingly negative upwelling temperature signatures to develop along the coastal with additional upwelling filaments at the center of the southwestern and southern tip of Sicily (Figures IV-18c to IV-21c). In addition, this period of multiple coastal upwelling filaments occurs with a less coherent ABV. Looking at available wind data, the weakening of the upwelling filament off the western tip of Sicily occurs when winds shift from northerly to onshore winds, agreeing with observations by Robinson et al. (1999). The increased coastal upwelling and multiple offshore filaments develop when winds shift from onshore (southwesterly) to north northwesterly. Finally the upwelling filament off the western tip of Sicily strengthens, while the remaining southwestern coast of Sicily experiences reduced upwelling anomalies.

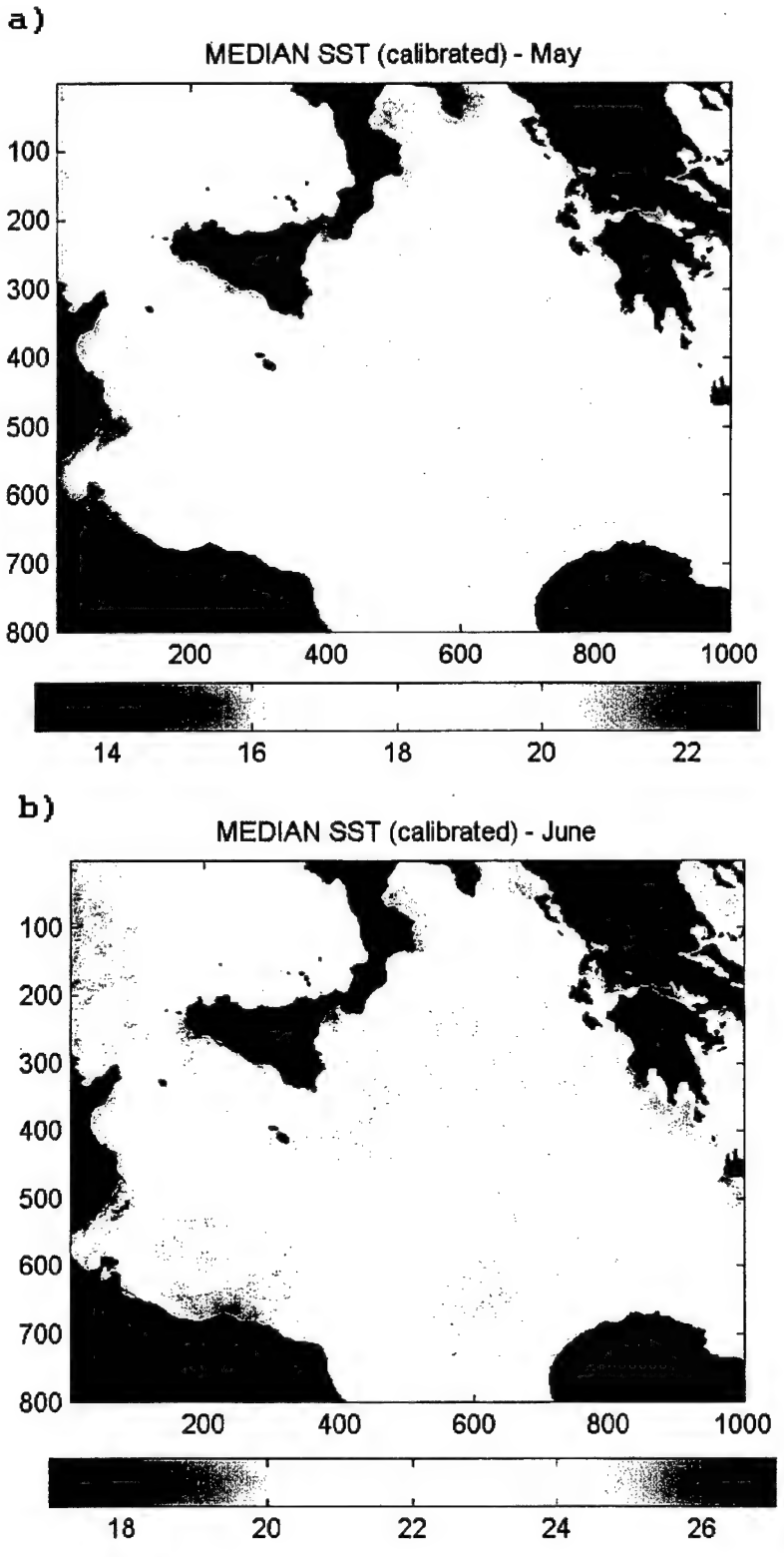

Figure IV-2. Median temperature composites for (a) May and (b) June, 1995.

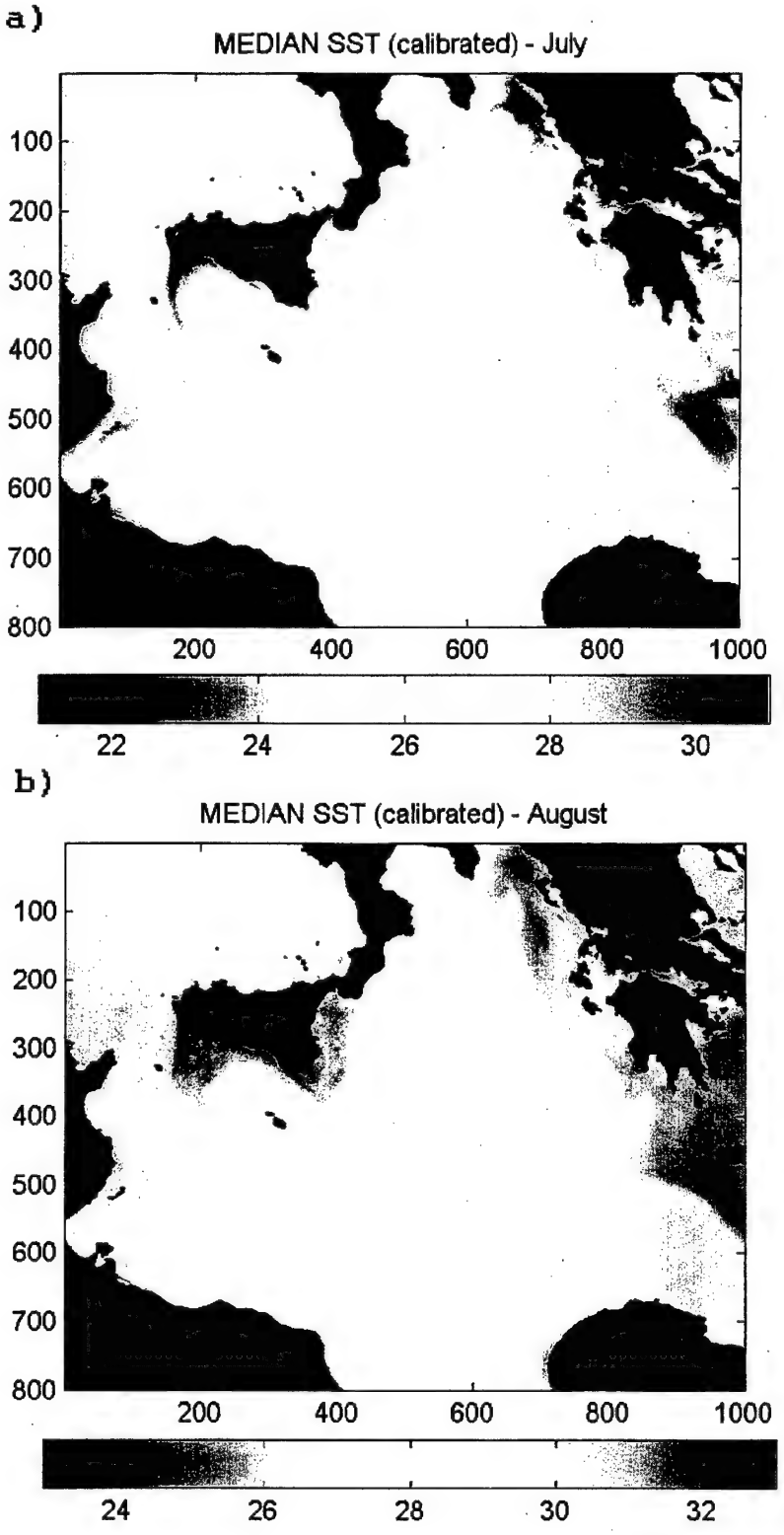

Figure IV-3. Median temperature composites for (a) July and (b) August, 1995.

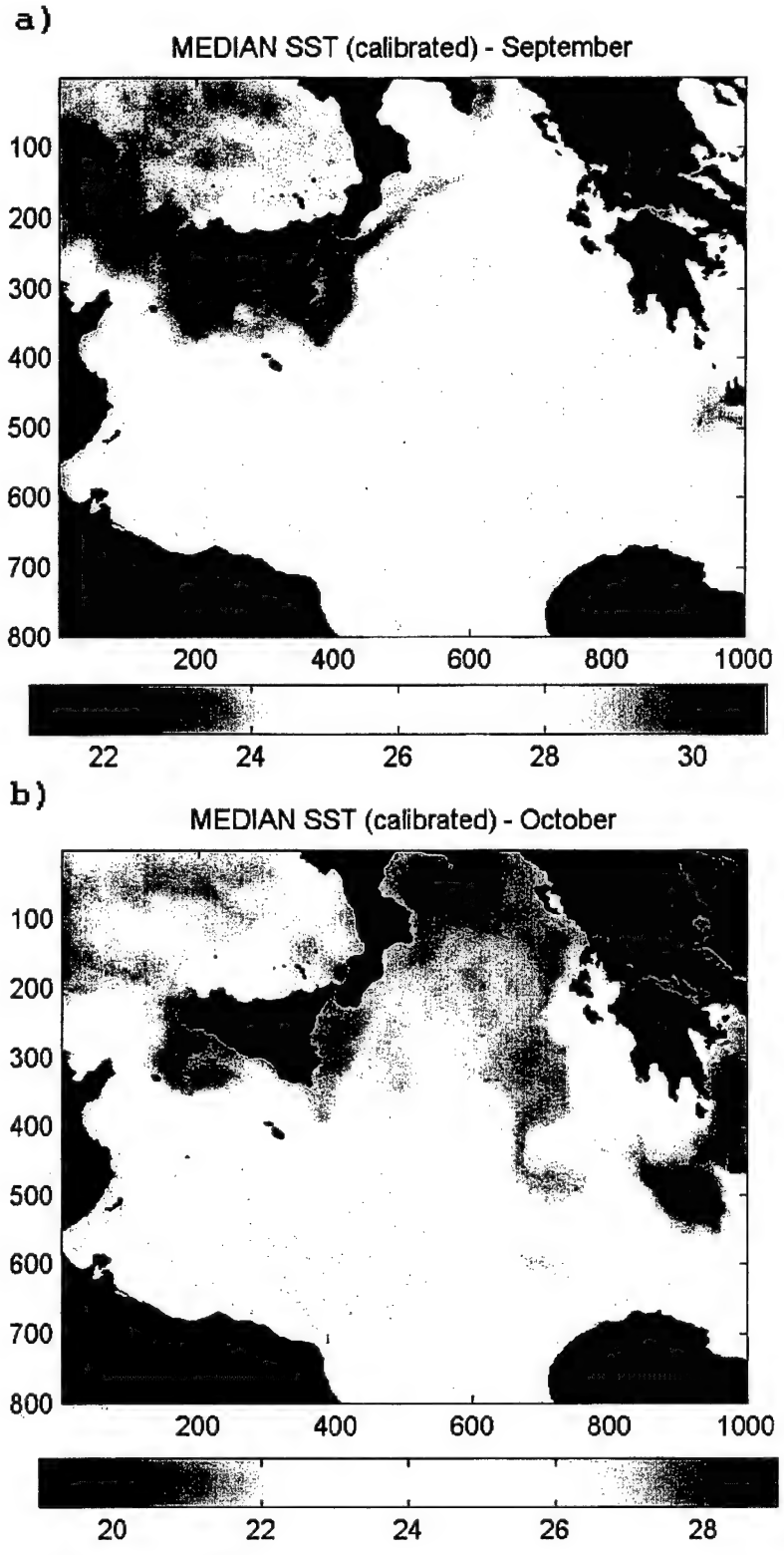

Figure IV-4. Median temperature composites for (a) September and (b) October, 1995.

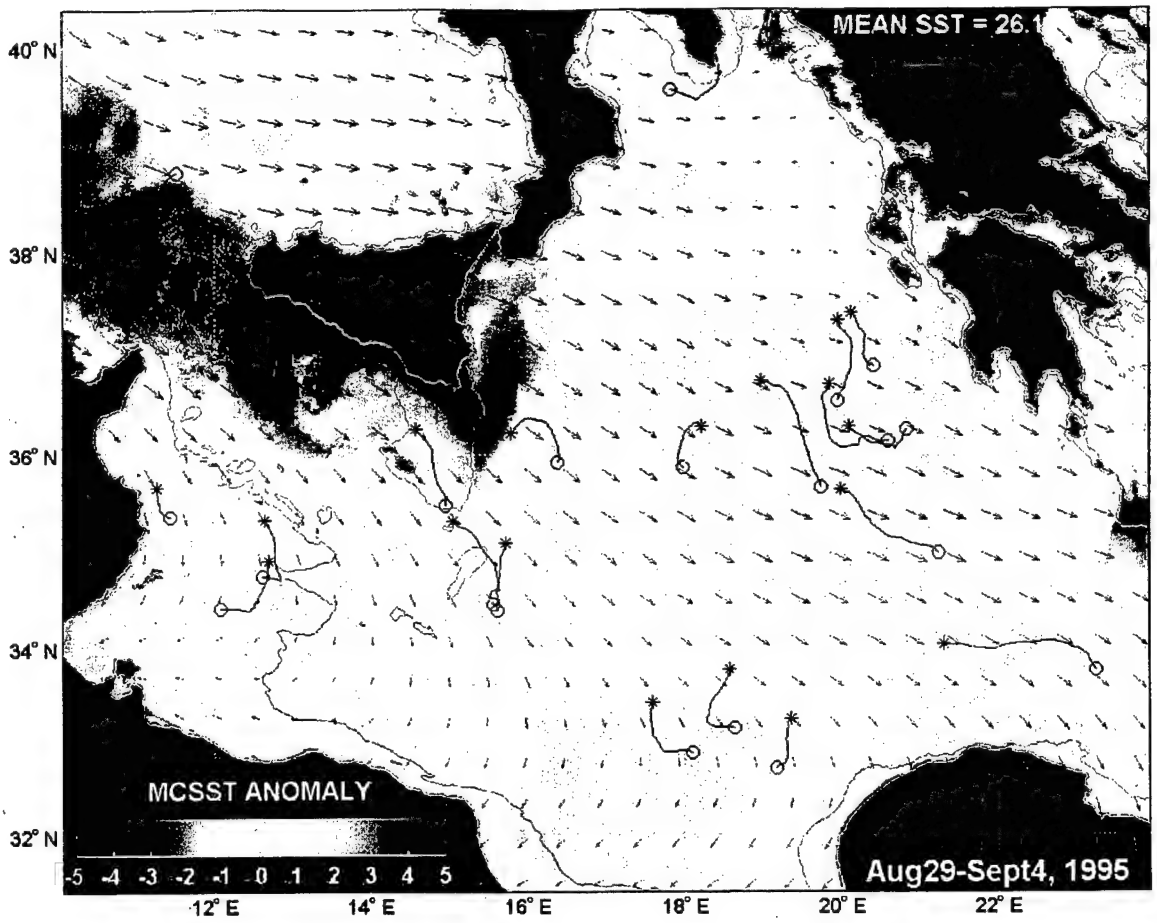

Figure IV-5. Composite map of mean SST anomaly of the median SST for the week of August 29 to September 4, 1995. Overlaid is the weekly summary of rotated NORAPS winds showing surface direction and speed. Also shown are 10-day long drifter trajectory segments centered on the week considered.

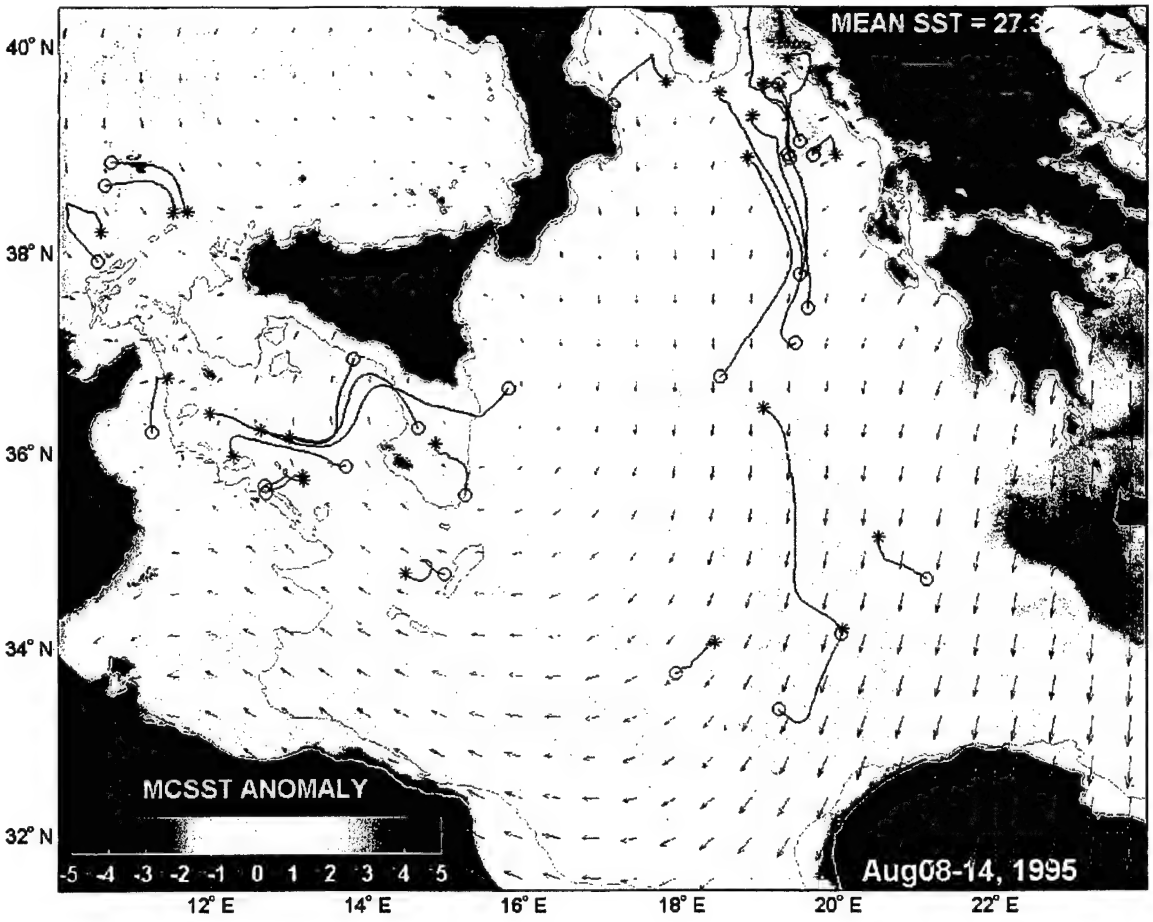

Figure IV-6. Composite map of mean SST anomaly of the median SST for the week of August 8 to 14, 1995. Overlaid is the weekly summary of rotated NORAPS winds showing surface direction and speed. Also shown are 10-day long drifter trajectory segments centered on the week considered.

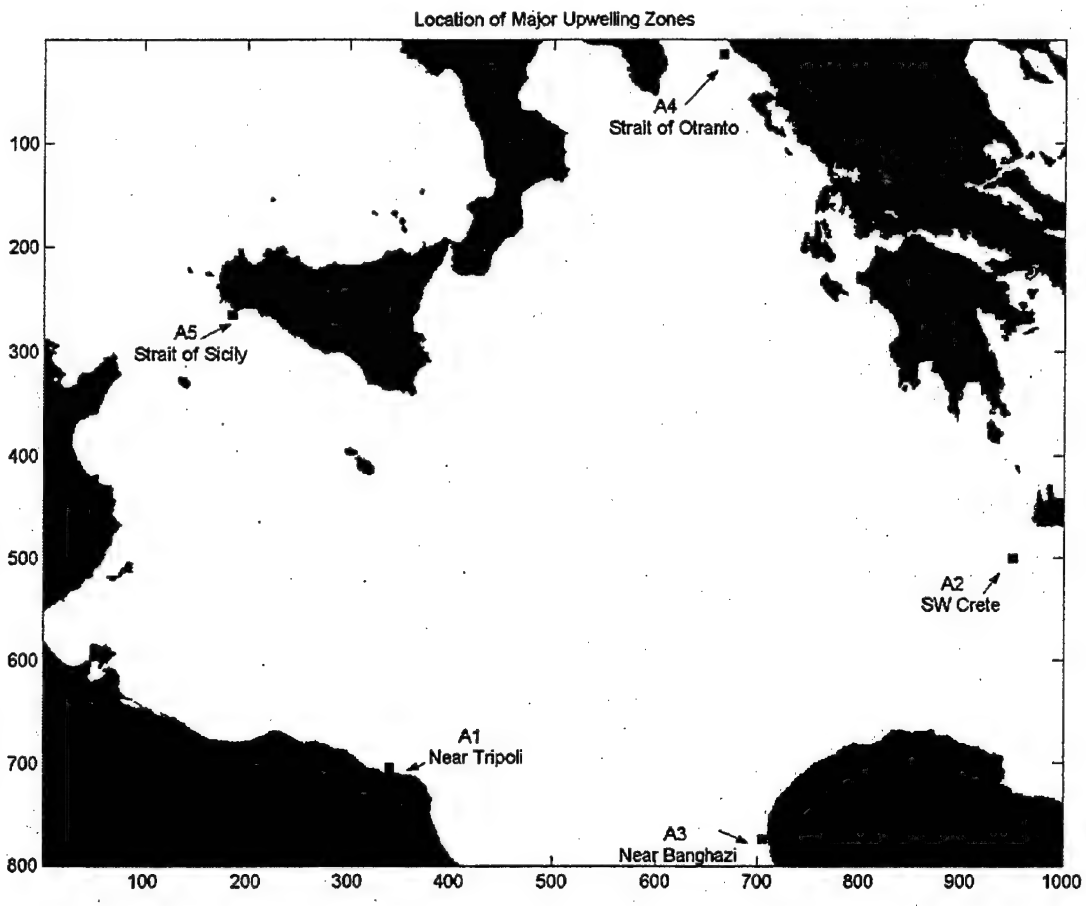

Figure IV-7. Location of major upwelling areas in the Ionian Sea.

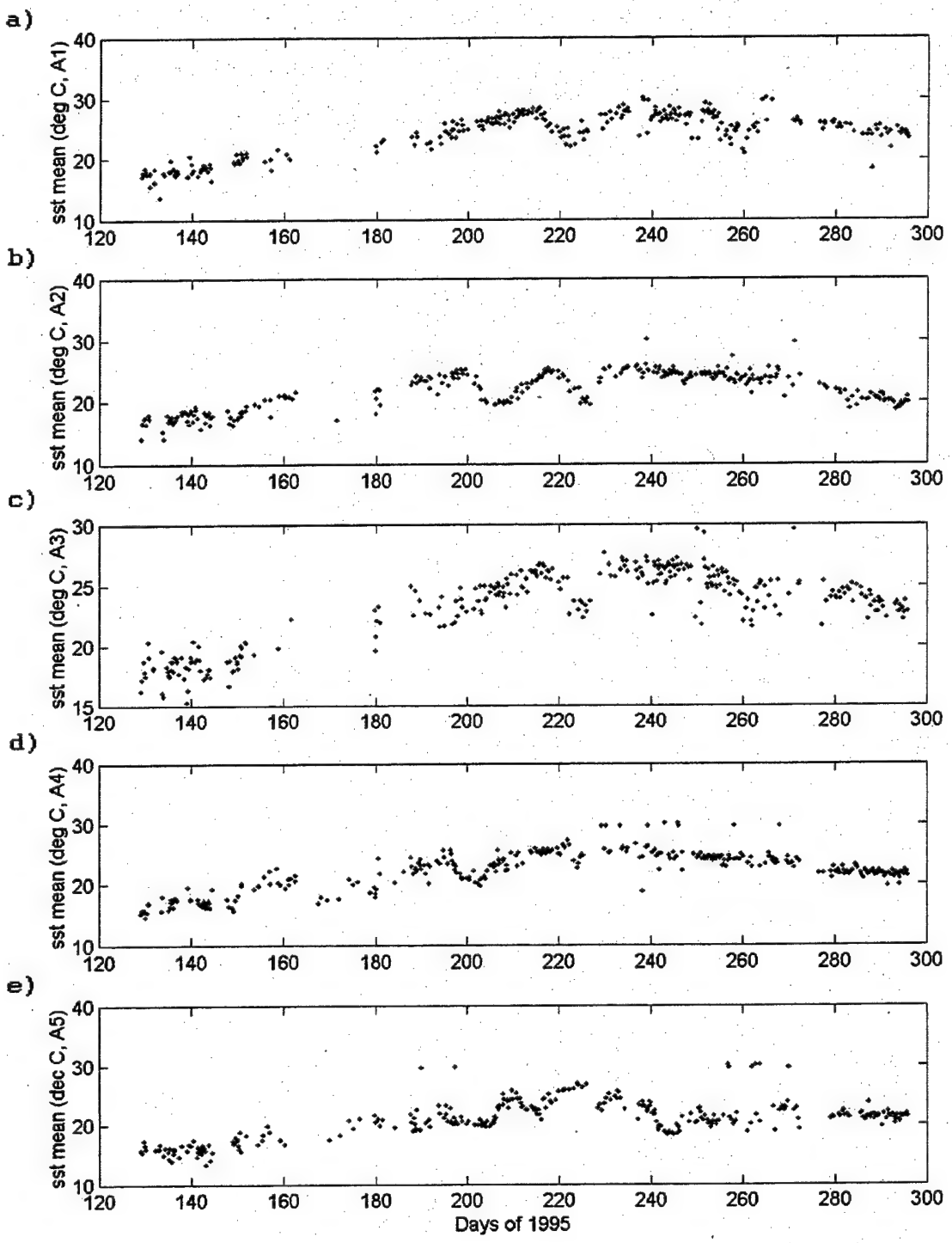

Figure IV-8. Plot of SST mean of weekly-median SST composites for July to September, 1995, for areas of upwelling (a, b, c, d and e).

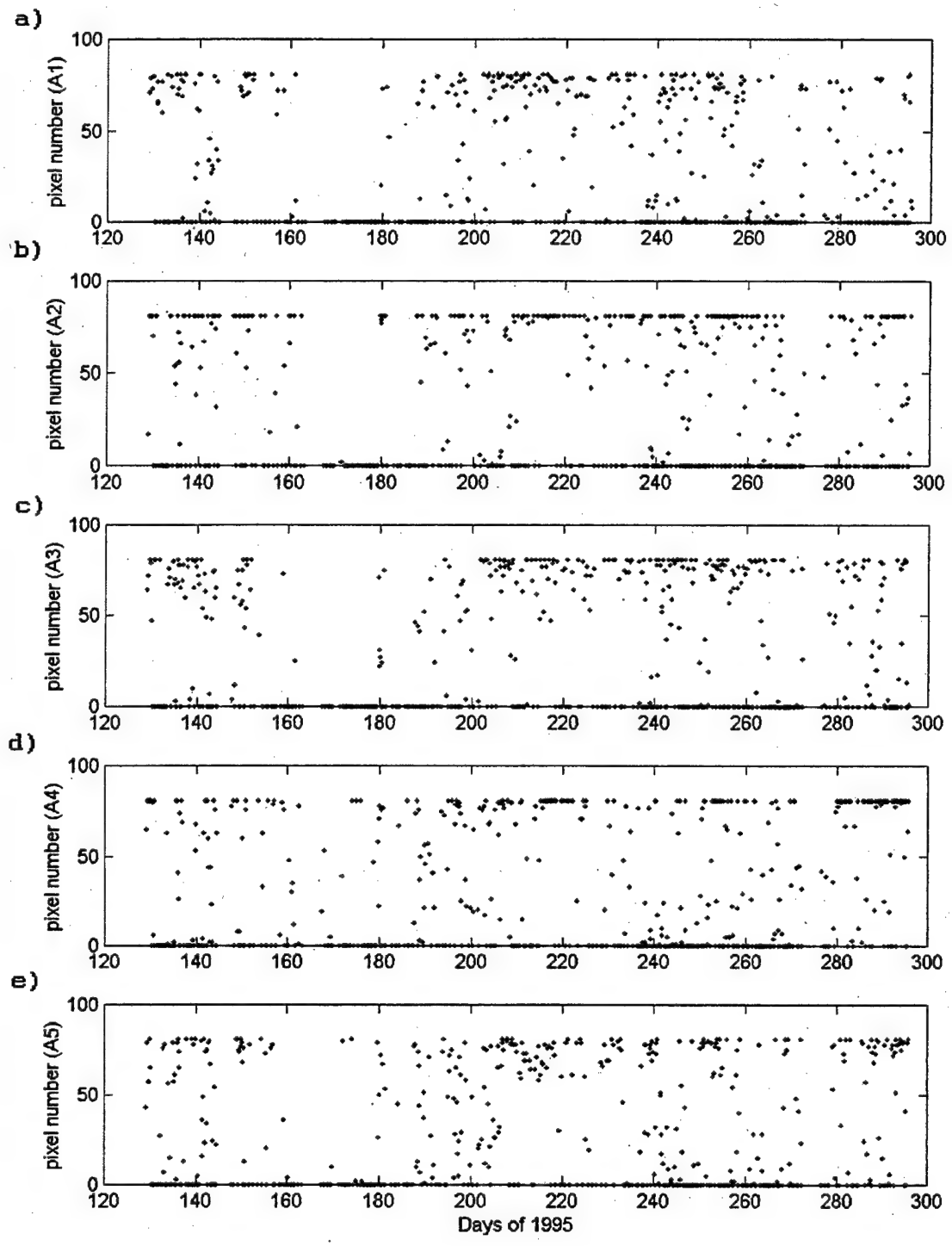

Figure IV-9. Plot of number of non-contaminated pixels (in 9x9-pixel area) from the weekly-median SST composites for July to September, 1995, for areas of upwelling (a, b, c, d and e).

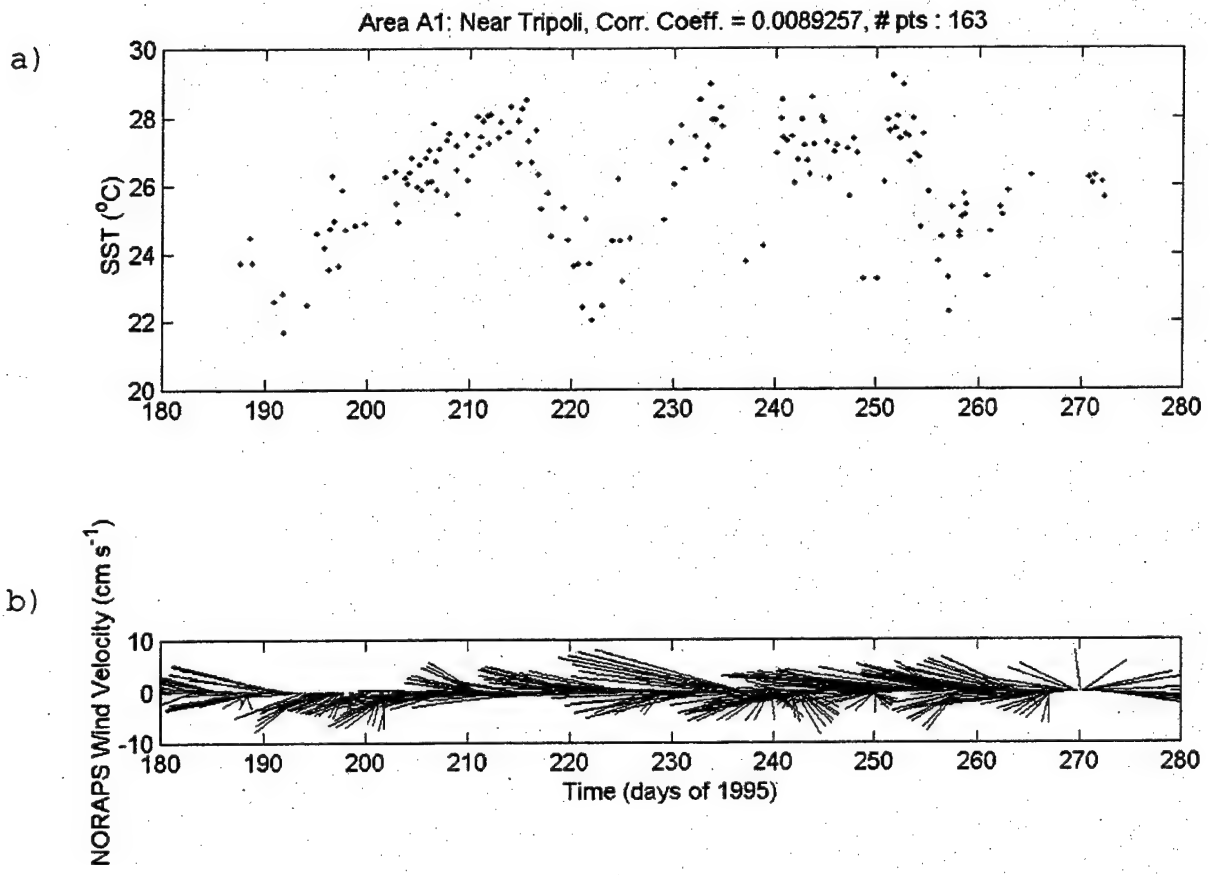

Figure IV-10. Plot of (a) sea surface temperature at area A1 (near Tripoli) and (b) wind vectors from NORAPS data for the period July to September, 1995.

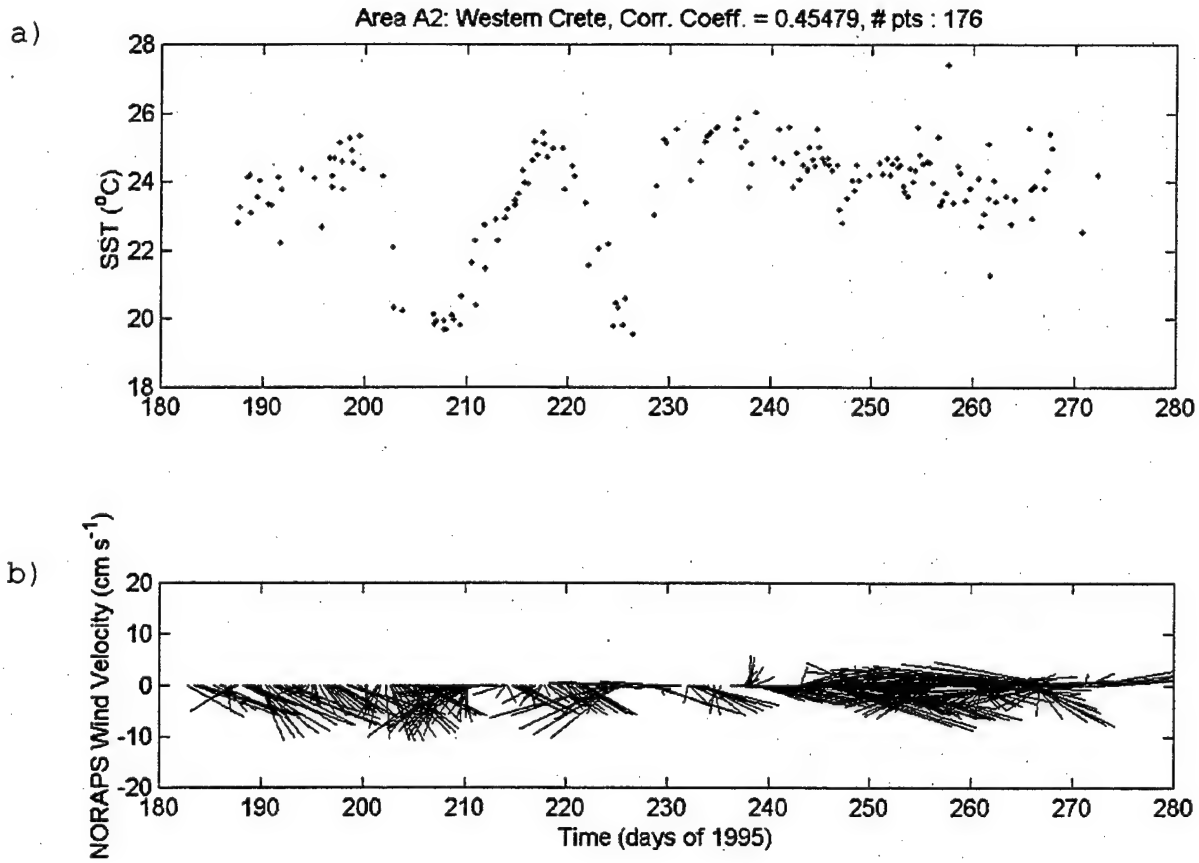

Figure IV-11. Plot of (a) sea surface temperature at area A2 (near western Crete) and (b) wind vectors from NORAPS data for the period July to September, 1995.

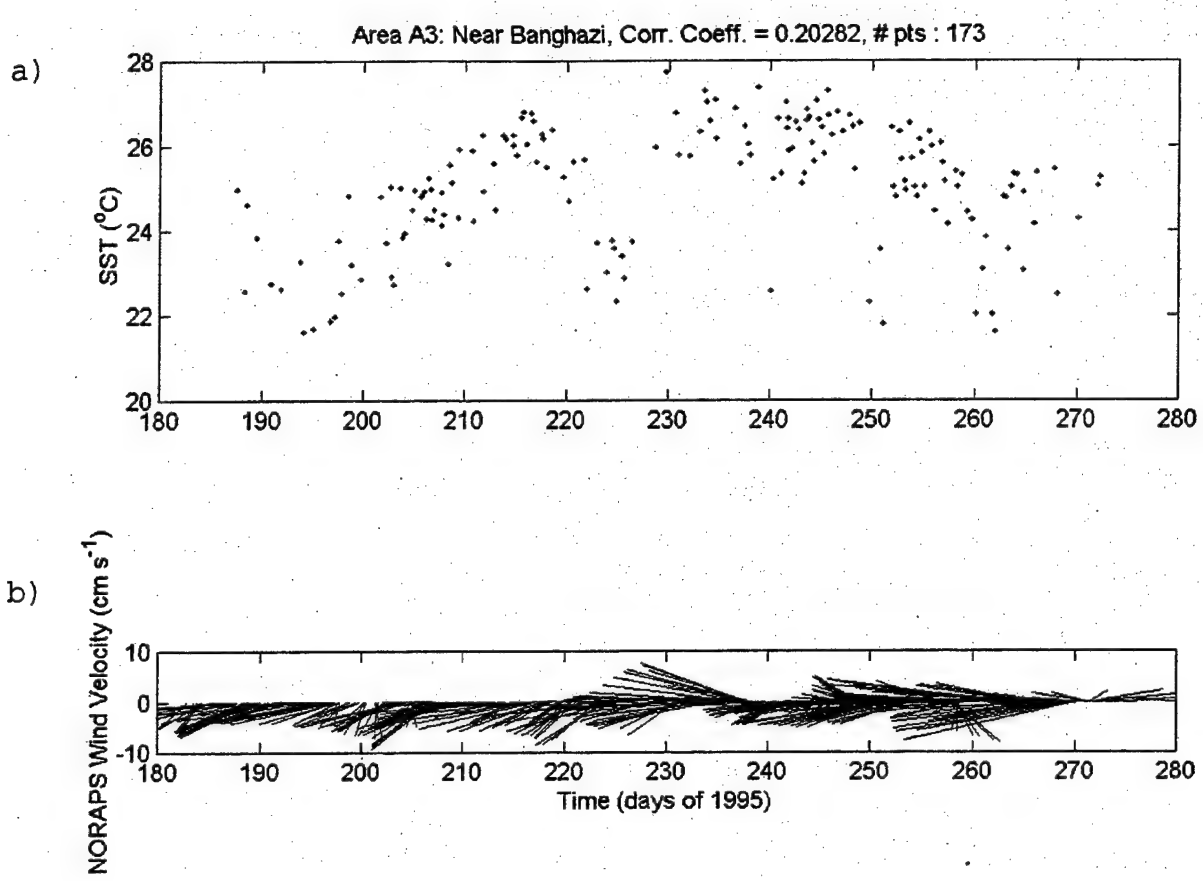

Figure IV-12. Plot of (a) sea surface temperature at area A3 (near Banghazi) and (b) wind vectors from NORAPS data for the period July to September, 1995.

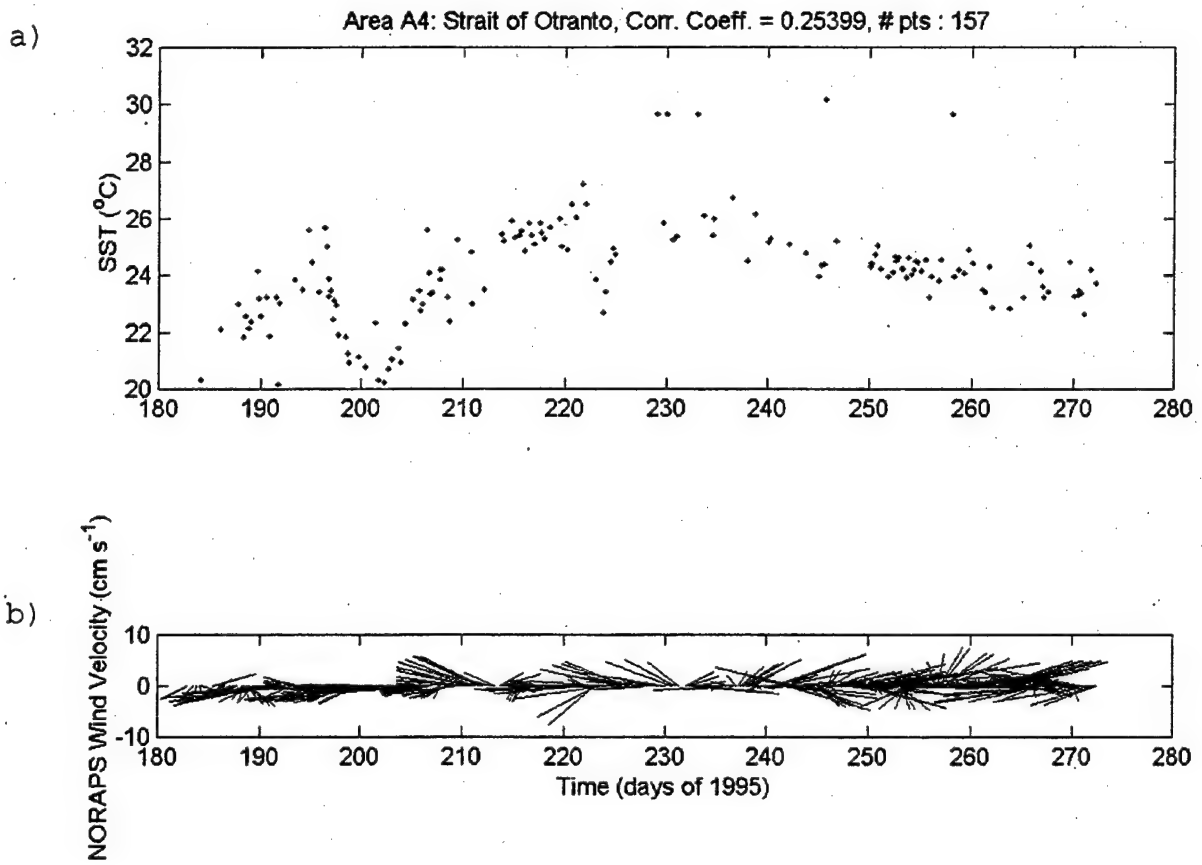

Figure IV-13. Plot of (a) sea surface temperature in area A4 (eastern Strait of Otranto) and (b) wind vectors from NORAPS data for the period July to September, 1995.

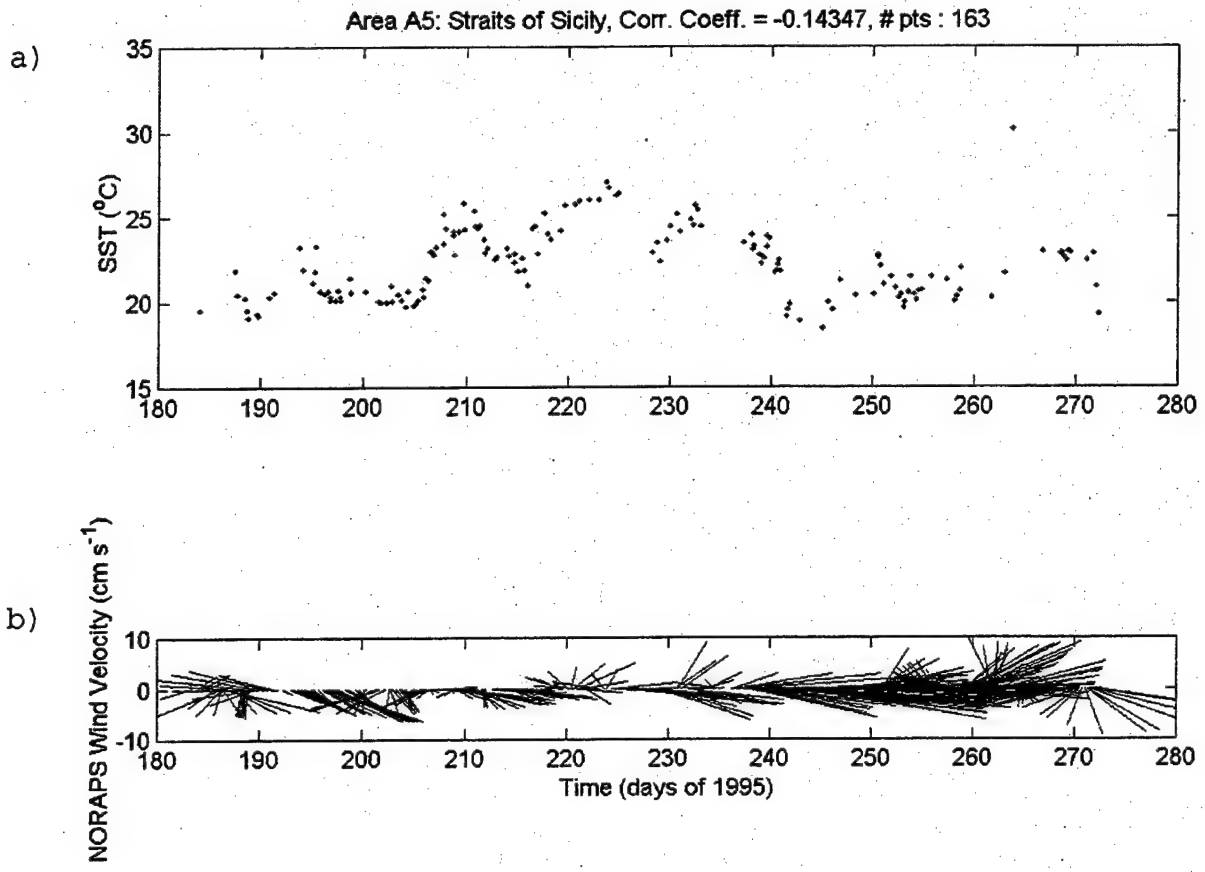

Figure IV-14. Plot of (a) sea surface temperature in area A5 (in Strait of Sicily) and (b) wind vectors from NORAPS data for the period July to September, 1995.

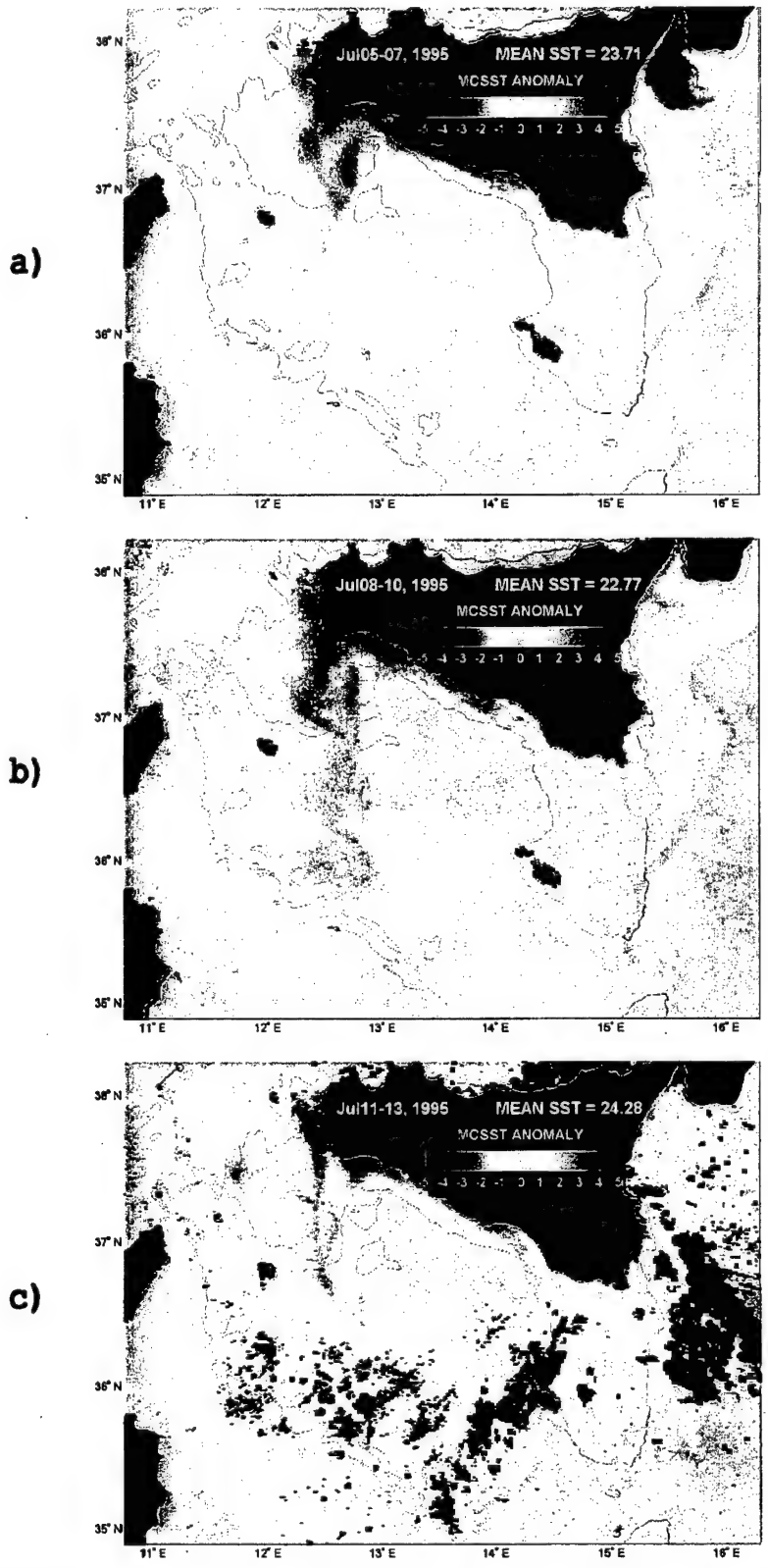

Figure IV-15. Three-day composites of SST anomaly for (a) 5-7 July, (b) 8-10 July and (c) 11-13 July, 1995. 5-day long drifter trajectories centered on the 3-day periods are overlaid on the images.

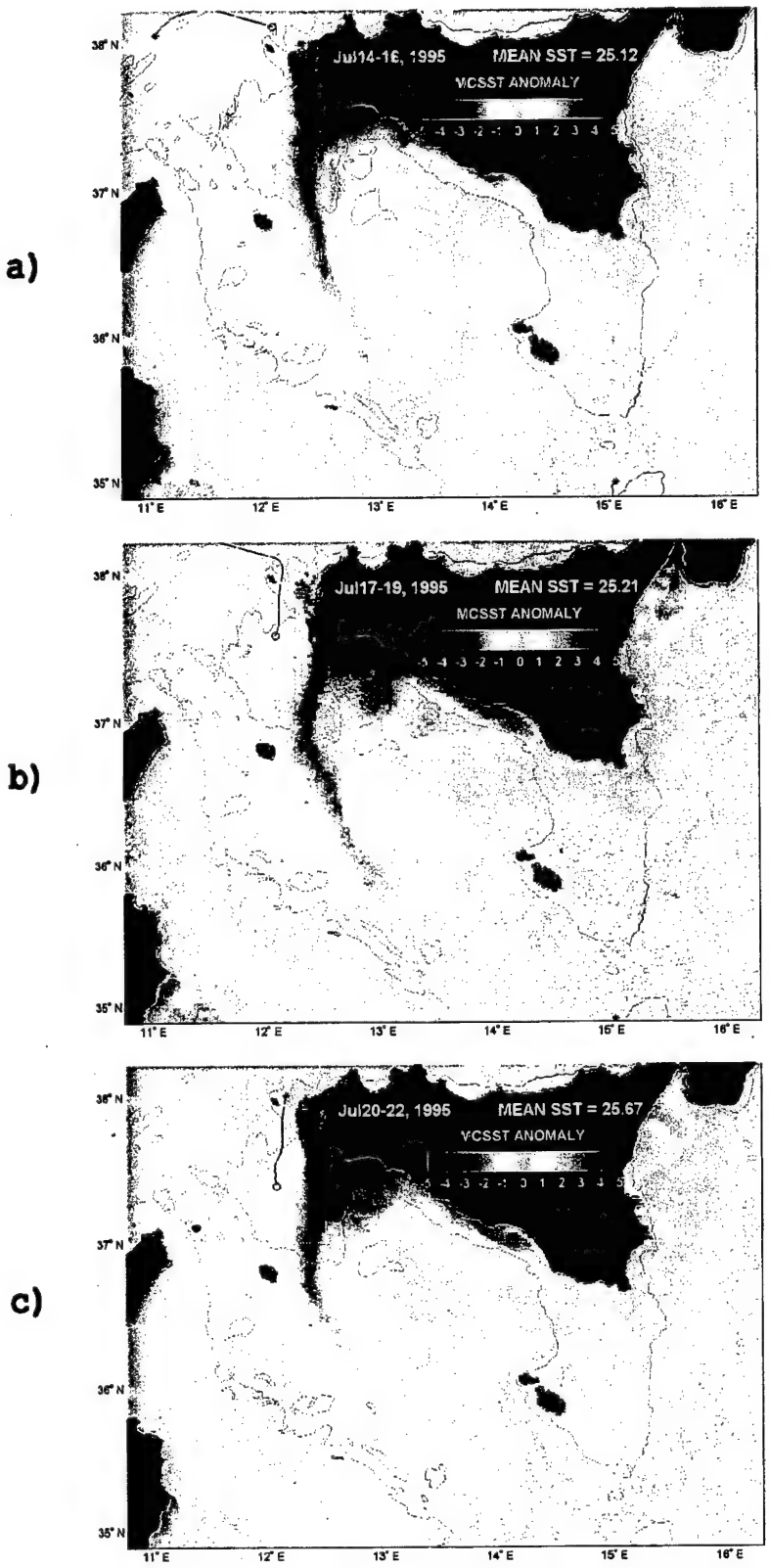

Figure IV-16. Three-day composites of SST anomaly for (a) 14-16, (b) 17-19 and (c) 20-22 July, 1995. 5-day long drifter trajectories centered on the 3-day periods are overlaid on the images.

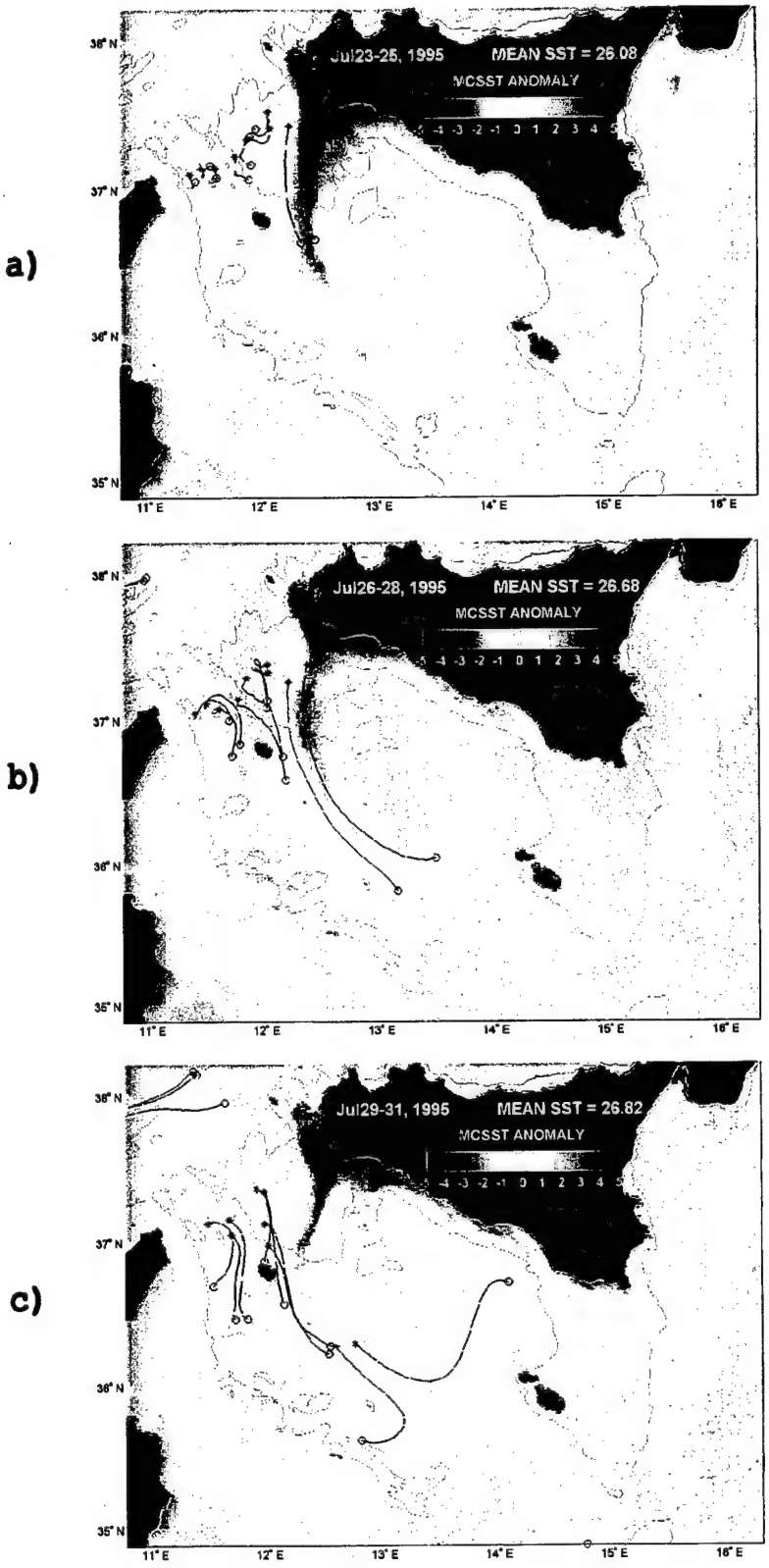

Figure IV-17. Three-day composites of SST anomaly for (a) 23-25, (b) 26-28 and (c) 29-31 July, 1995. 5-day long drifter trajectories centered on the 3-day periods are overlaid on the images.

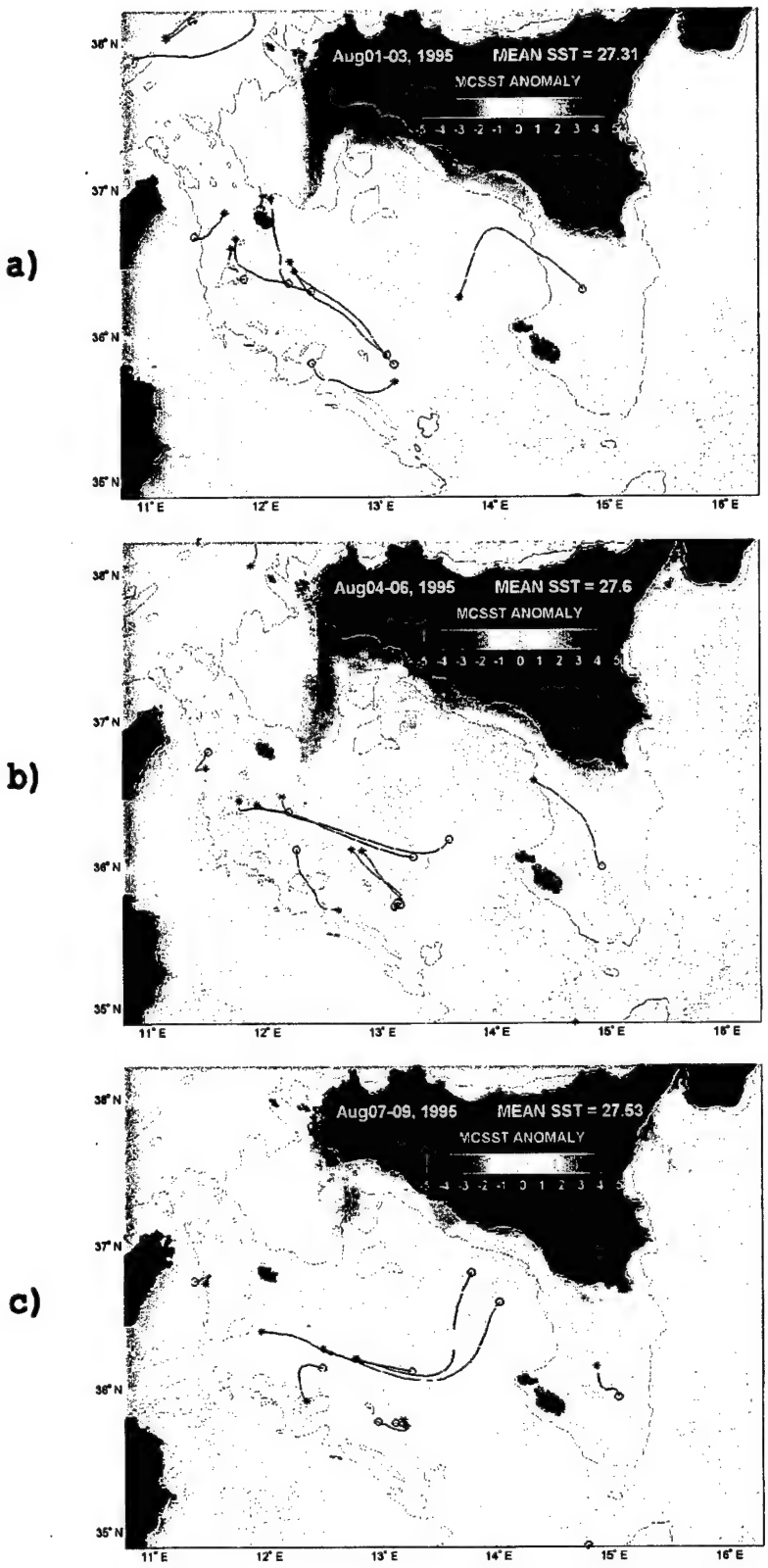

Figure IV-18. Three-day composites of SST anomaly for (a) 1-3, (b) 4-6 and (c) 7-9 August, 1995. 5-day long drifter trajectories centered on the 3-day periods are overlaid on the images.

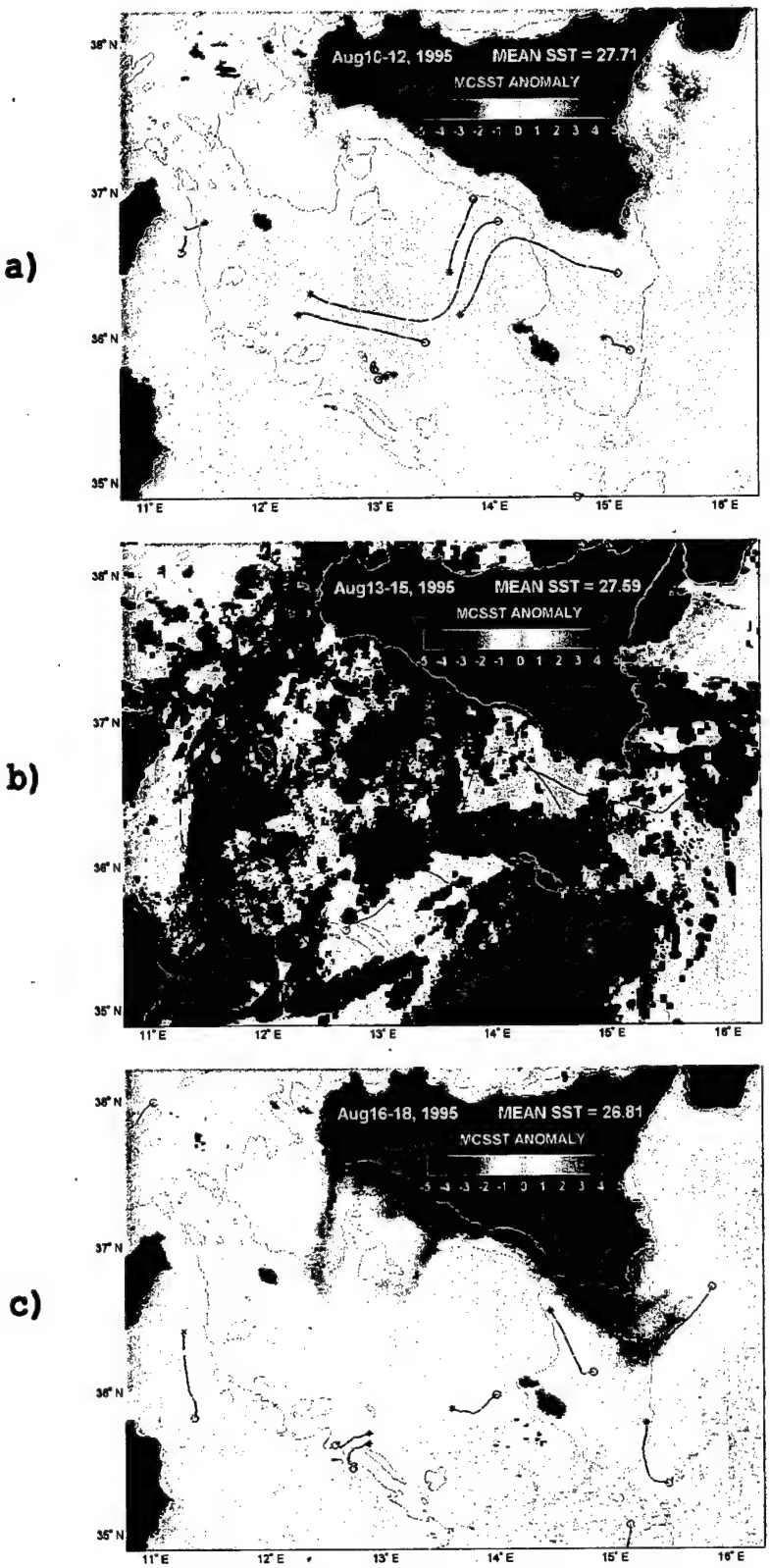

Figure IV-19. Three-day composites of SST anomaly for (a) 10-12, (b) 13-15 and (c) 16-18 August, 1995. 5-day long drifter trajectories centered on the 3-day periods are overlaid on the images.

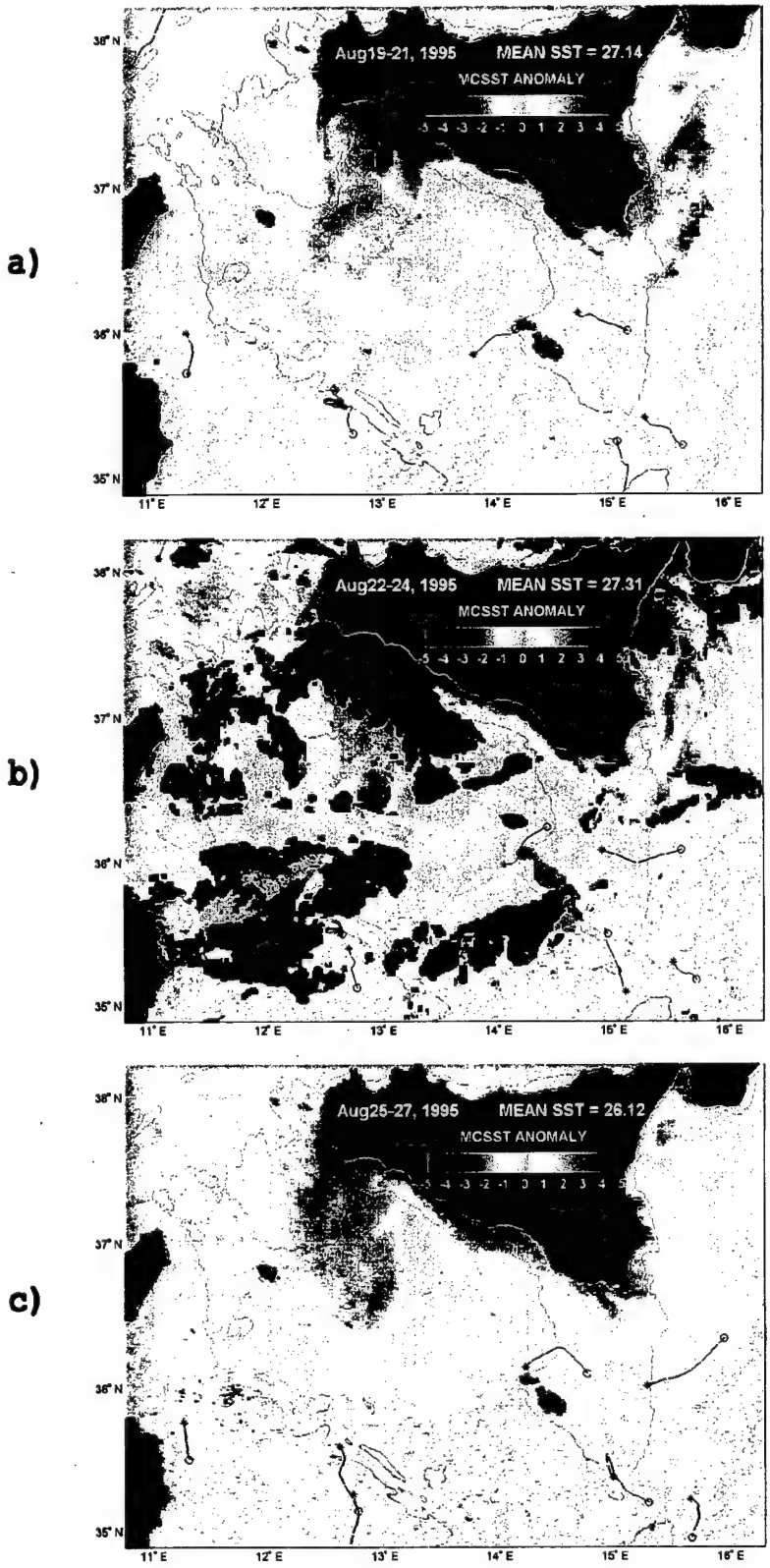

Figure IV-20. Three-day composites of SST anomaly for (a) 19-21, (b) 22-24 and (c) 25-27 August, 1995. 5-day long drifter trajectories centered on the 3-day periods are overlaid on the images.

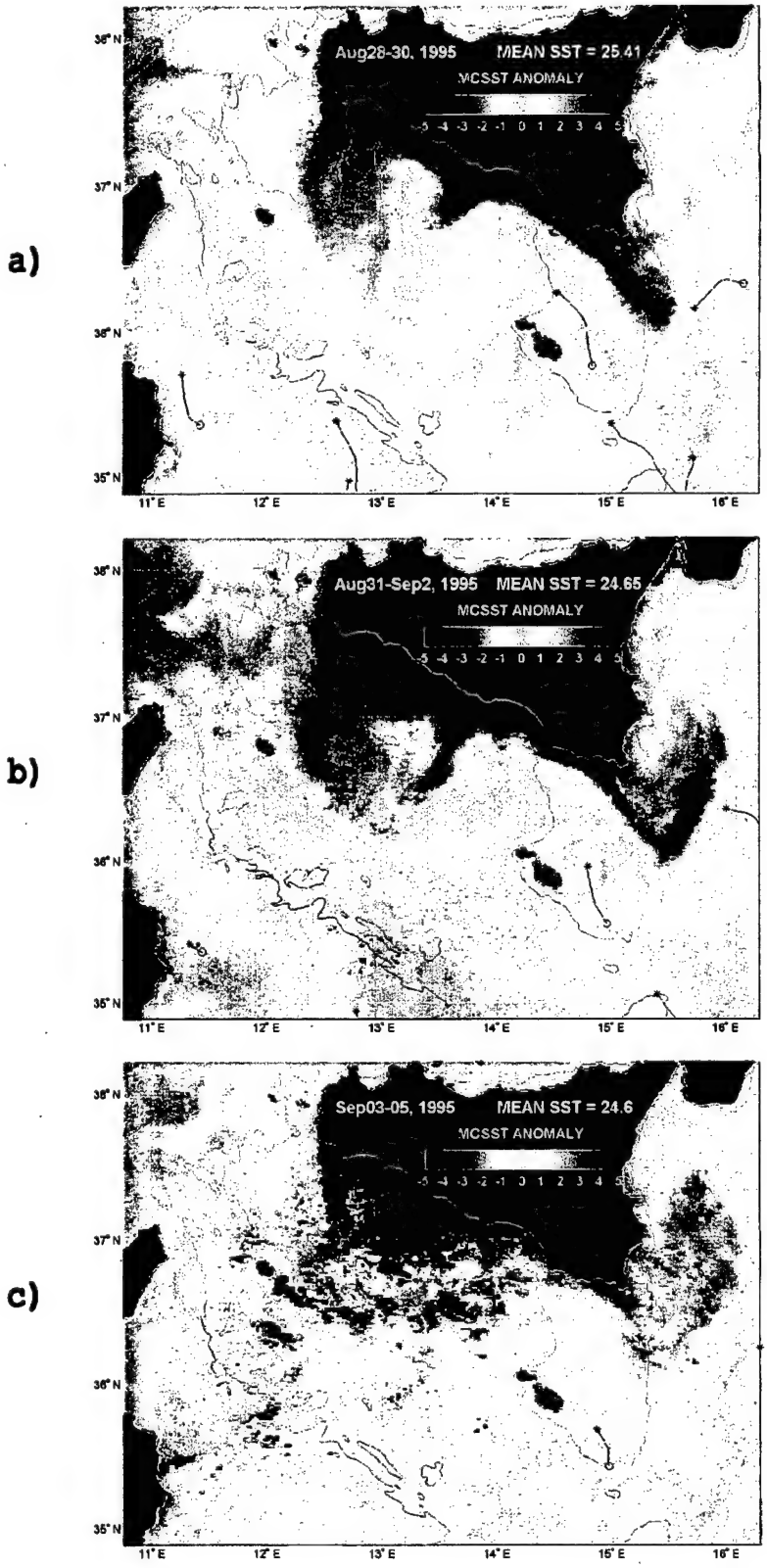

Figure IV-21. Three-day composites of SST anomaly for (a) 28-30 August, (b) 31 August-2 September and (c) 3-5 September, 1995. 5-day long drifter trajectories centered on the 3-day periods are overlaid on the images.

V. DISCUSSION AND CONCLUSIONS

This study examined the mesoscale and sub-basin sea surface temperature structures of the Ionian Sea to characterize and compare temporal and seasonal variability with previous observations, for the time period between May and October, 1995. Using full spatial resolution (1.25x1.25 km) of satellite AVHRR images, satellite data were compared with simultaneous and collocated in situ drifter data to generate bias that could be applied to all images from the time period being studied. A maximum temperature bias of 1.14 °C was calculated. Corrected satellite AVHRR images were combined over one-day, three-day, weekly and monthly time periods to generate composite images of the median sea surface temperature for the Ionian Sea from non-contaminated day/night image pixels. Selected SST composites were over-laid with drifter tracks and wind vectors for comparing the thermal features with the surface currents and the wind forcing. While the diurnal cycle is recognized as a source of error to the compositing technique used for analysis in this study (1-2 °C), it was not possible to correct for it with the available data.

For the time period (May to October, 1995) of this study, seasonal variability compares favorably with the

observations of previous studies of the Ionian Sea. Agreeing with the observations of Marullo et al. (1999) and Philippe and Harang (1982), the transitional months of May, September and October show a distinct zonal SST pattern, with cool and warm waters located in the northern and southern Ionian, respectively. This cycles to the summer months, with large areas of warm water dominating the interior of the Ionian. These results compare favorably with the observations by Marullo et al. (1999, see Figure III-4). However, a direct comparison of sub-basin thermal features is impossible due to the lower spatial resolution (18x18 km) used to produce the decade composite. The spatial and temporal variability of sub-basin features (e.g., upwelling events, cold cyclones and basin-wide SST warming) is much clearer in our monthly (Figures IV-2 to IV-4) and weekly composites.

A number of coastal locations throughout the Ionian are sites of wind driven upwelling events, with the Strait of Sicily having the most consistently apparent signature. The presence of sub-basin and mesoscale structures is also a significant characteristic of the Ionian Sea. The AIS follows a predictable path between Sicily and Malta, turning northeast towards the Strait of Otranto, then heading south along the Greek coast as the MMJ, before

entering the Levantine Sea through the Cretan Passage. The Cretan Cyclone is a feature that exists in some form during the period of study, with increased temperature signature in the presence of northerly Etesian winds. Also, the warm Pelops Anticyclone southwest of Greece is not detected in the SST composites during the period of investigation.

The use of various time periods for creating composite images shows the differences between what can be examined depending of the time scale of the variability. While one-day and three-day composites can detail the formation of small gyres, like the Adventure Bank Vortex, and movement of cool water from the Atlantic to the Ionian through the Strait of Messina, weekly and monthly composites smooth over these short temporal anomalies. On the other hand, weekly and monthly composites can illustrate variations of sea surface temperature over a seasonal cycle, allowing trends to be predicted. The SST composites delineate satisfactorily the sub-basin thermal features in the Ionian Sea for the oceanographer (e.g., AIS, MMJ and Cretan Cyclone).

VI. RECOMMENDATIONS

The comparisons between AVHRR images and co-temporal and collocated in situ drifter data suggests that the general MCSST coefficients might be augmented with localized biases when more accurate sea surface temperatures are desired. Also, the utilization of the full spatial resolution of the AVHRR images in combination with short compositing time periods allows the more precise identification of sub-basin and mesoscale sea surface temperature features. By automation of this data processing from multiple sources, a useful product could be produced for a variety of applications.

LIST OF REFERENCES

Anonymous, "Adriatic Sea; Sea Surface Temperature Images from the NOAA Advanced Very High Resolution Radiometer 9 May to 22 October," IFREMER CD-ROM, 1998.

Briscoe, M.G., O.M. Johannssen, and S. Vincenzi, "The Maltese oceanic front: a surface description by ship and aircraft," Deep-Sea Res., 21: 247-262, 1974.

Bohm, E. and E. Salusti, "Satellite and field observations of currents on the eastern Sicilian Shelf," *Remote Sensing of the Shelf Sea Hydrodynamics*, 38: 51-68, Elsevier, New York, 1984.

Gacic, M., S. Marullo, R. Santoleri, and A. Bergamasco, "Analysis of the seasonal and interannual variability of the sea surface temperature field in the Adriatic Sea from AVHRR data (1984-1992)," J. Geophys. Res., 102(C10), 22937-22946, 1997.

Godfrey, J.S. and M. Tomaczak, *Regional Oceanography: An Introduction*, p. 89, Pergamom, New York, 1994.

Horton, C., M. Clifford, J. Schmitz, "A real-time oceanographic nowcast/forecast system for the Mediterranean Sea," J. Geophys. Res., 102 (C11), 25123-25156, 1997.

Huxley, A., *Standard Encyclopedia of the World's Oceans and Islands*, p. 165, 207-209, Putnam, New York, 1962.

Lillesand, T.M. and R.W. Kiefer, *Remote Sensing and Image Interpretation*, p. 498-500, Wiley, New York, 1994.

Malanotte-Rizzoli, P., B.B. Manca, M.R. D'Alcala, A. Theocharis, A. Bergamasco, D. Bregant, G. Budillon, G. Civitarese, D. Georgopoulos, A. Michelato, E. Sansone, P. Scarazzato, and E. Souvermezoglou, "A synthesis of the Ionian Sea hydrography, circulation and water mass pathways during POEM-Phase I," Prog. Oceanogr., 39: 153-204, 1997.

Manzella, G.M.R., T.S. Hopkins, P.J. Minnett, and E. Nacini, "Atlantic Water in the Strait of Sicily," J. Geophys. Res., 95: 1569-1575, 1990.

Marullo, S., R. Santoleri, P. Malanotte-Rizzoli, and A. Bergamasco, "The sea surface temperature field in the Eastern Mediterranean from advanced very high resolution radiometer (AVHRR) data, Part II. Interannual variability," J. Mar. Syst., 20: 83-112, 1999.

Matteoda, A. and S.M. Glenn, "Observations of recurrent mesoscale eddies in the eastern Mediterranean," J. Geophys. Oceanogr., 101: 20,687-20,709, 1996.

McClain, E.P., W.G. Pichel, and C.C. Walton, "Comparative performance of AVHRR-based multichannel sea surface temperature," J. Geophys. Res., 90(C6), 11,587-11,601, 1985.

Philippe, M. and L. Harang, "Surface temperature fronts in the Mediterranean Sea from Infrared Satellite Imagery," Hydrodynamics of Semi-enclosed Seas, 91-128, Elsevier, 1982.

Pickard, G.L. and W.J. Emery, *Descriptive Physical Oceanography: An Introduction*, pp. 208, Pergamom, Boston, 1990.

Poulain, P.-M., "Lagrangian Measurements of Surface Circulation in the Adriatic and Ionian Seas between November 1994 and March 1997," Rapp. Comm. Int. Mer. Medit., 35: 190-191, 1998.

Poulain, P.-M., "Drifter observations of surface circulation in the Adriatic Sea between December 1994 and March 1996," J. Mar. Syst., 20: 231-253, 1999.

Robinson, A.R., J. Sellschopp, A. Warn-Varns, W.G. Leslie, C.J. Lozano, P.J. Haley Jr., L.A. Anderson and P.F.J. Lermusiaux, "The Atlantic Ionian Stream," J. Mar. Syst., 20: 129-156, 1999.

Roether, W., B. Klein, V. Beitzel, B.B. Manca, "Property distributions and transient-tracer ages in Levantine Intermediate Water in the Eastern Mediterranean," J. Mar. Syst., 18:71-87, 1998.

Strong, A.E. and E.P. McClain, "Improved ocean surface temperatures from space-comparisons with drifting buoys," Bull. Amer. Meteor. Soc., vol. 65, pp. 138-142, 1984.

INITIAL DISTRIBUTION LIST

1. Defense Technical Information Center 2
   8725 John J. Kingman Road, STE 0944
   Ft. Belvoir, Virginia 22060-6218

2. Dudley Knox Library 2
   Naval Postgraduate School
   411 Dyer Rd.
   Monterey, California 93943-5101

3. Chairman, Code OC 1
   Department of Oceanography
   Naval Postgraduate School
   833 Dyer Rd. Room 328
   Monterey, California 93943-5122

4. Professor Pierre-Marie Poulain (Code OC/PN) 4
   Department of Oceanography
   Naval Postgraduate School
   833 Dyer Rd. Room 328
   Monterey, California 93943-5122

5. Professor Philip A. Durkee (Code MR/DE). 1
   Department of Meteorology
   Naval Postgraduate School
   Monterey, California 93943

6. Professor Pierre Flament 1
   Department of Oceanography
   University of Hawaii
   1000 Pope Road
   Honolulu, Hawaii 96822

7. Director 1
   SACLANT Undersea Research Centre
   SACLANTCEN CMR 426
   APO-AE 09613-5000

8. LT Jeff M. Leitz 2
   1408 San Cristobal Ave #2
   Port Charlotte, Fl 33983